Digital Comprehensive Summaries of Uppsala Dissertations
from the Faculty of Science and Technology 2339

Advancements in Lithium-Based Batteries

Unraveling and Mitigating Performance-Limiting Phenomena in Negative Electrodes

YU-KAI HUANG

ACTA UNIVERSITATIS
UPSALIENSIS
2023

ISSN 1651-6214
ISBN 978-91-513-1967-4
urn:nbn:se:uu:diva-516251

UPPSALA
UNIVERSITET

Dissertation presented at Uppsala University to be publicly examined in Room Sonja Lyttkens, Ångströmlaboratoriet, Lägerhyddsvägen 1, Uppsala, Friday, 12 January 2024 at 09:15 for the degree of Doctor of Philosophy. The examination will be conducted in English. Faculty examiner: PD Dr. Gunther Brunklaus (Forschungszentrum Jülich GmbH).

Abstract

Huang, Y.-K. 2023. Advancements in Lithium-Based Batteries. Unraveling and Mitigating Performance-Limiting Phenomena in Negative Electrodes. *Digital Comprehensive Summaries of Uppsala Dissertations from the Faculty of Science and Technology* 2339. 72 pp. Uppsala: Acta Universitatis Upsaliensis. ISBN 978-91-513-1967-4.

The development of lithium-based batteries, especially lithium-ion batteries, has changed our daily lives significantly. The technologies first enabled by lithium-based batteries are now in turn creating a demand for better lithium-based batteries with higher energy densities and longer cycling lifetimes. This requires studies and development of negative electrodes, with a particular focus on gaining a better and more complete understanding of all performance-limiting phenomena and to develop appropriate mitigation strategies.

For negative electrodes based on alloy-forming materials such as silicon, aluminum and tin, it has, recently been shown that capacities losses can result from diffusion-controlled trapping of lithium due to an incomplete delithiation of the electrodes. In the first part of the thesis, it is demonstrated explicitly that such a lithium trapping effect also is seen for conventional graphite electrodes. This effect is further demonstrated to greatly affect the cycle life performance of NMC811/graphite full cells during high-rate cycling. However, it is also demonstrated that the inclusion of constant-voltage delithiation steps can increase the delithiation efficiency and decrease the influence of the trapping effect. The use of silicon electrodes based on silicon nanoparticles is also revisited. It is proposed that the influence of the lithium trapping effect seen for such electrodes is affected by the size of the employed silicon nanoparticles, most likely, via its influence on the electrode microstructure.

Replacing the currently used negative electrodes with lithium-metal electrodes, especially in a “anode-free” configuration, can significantly increase the energy densities of lithium-based batteries due to the high capacity and low electrochemical potential of elemental lithium. However, the inhomogeneous lithium deposition and stripping greatly limit the cycling performance. In the second part of this thesis, strategies focusing on electrochemically controlling the nucleation and growth of lithium are proposed to improve the deposition of lithium on lithium-metal electrodes as well as directly on copper current collectors. In the former study, it is shown that forming a great number of homogeneously distributed nucleation sites across the entire electrode surface, via the introduction of a one-second long potentiostatic oxidation pulse, subsequently yields more homogeneous lithium deposition. In the second study, it is found that the nucleation of lithium on copper current collectors can be affected by the diffusion of lithium into the current collectors. It is also demonstrated that the influence of this effect can be decreased by chemically prelithiating the current collectors so that more homogeneous lithium deposition can be attained.

Keywords: lithium-based batteries, negative electrodes, negative electrode materials, lithium diffusion, lithium trapping, lithium electrodeposition

Yu-Kai Huang, Department of Chemistry - Ångström, Inorganic Chemistry, Box 538, Uppsala University, SE-751 21 Uppsala, Sweden.

ISSN 1651-6214
ISBN 978-91-513-1967-4
URN urn:nbn:se:uu:diva-516251 (http://urn.kb.se/resolve?urn=urn:nbn:se:uu:diva-516251)

To my family
and all the people that support me along the way

List of Papers

This thesis is based on the following Papers, which are referred to in the text by their Roman numerals.

I. **Huang, Y.-K.**, Pettersson, J., Nyholm, L. (2022) Diffusion-controlled Lithium Trapping in Graphite Composite Electrodes for Lithium-ion batteries. *Advanced Energy and Sustainability Research*, 3 (8), 2200042

II. **Huang, Y.-K.**, Thulin, C. J., Nyholm, L., Rehnlund, D. (2023) Early Mitigation of Diffusion-controlled Lithium Trapping for Improved High-rate Cycling of Lithium-ion Battery Cells. *Submitted manuscript*.

III. **Huang, Y.-K.**, Nyholm, L. (2023) Influence of the Particle Size on Diffusion-controlled Lithium Trapping in Silicon Nanoparticle Based Electrodes. *In manuscript.*

IV. **Huang, Y.-K.**, Pan, R., Rehnlund, D., Wang, Z., Nyholm, L. (2021) First-Cycle Oxidative Generation of Lithium Nucleation Sites Stabilizes Lithium-Metal Electrodes. *Advanced Energy Materials*, 11 (9), 2003674

V. **Huang, Y.-K.**, Chen, H., Nyholm, L. (2023) Influence of Lithium Diffusion into Copper Current Collectors on Lithium Electrodeposition in Anode-Free Lithium-Metal Batteries. *Small*, 19 (43), 2306829

Disclaimer: Parts of this thesis are based on my licentiate thesis titled “Towards better anode materials for lithium-based batteries: lithium deposition and diffusion-controlled lithium trapping” (Uppsala University, 2022).

My contribution to the Papers:

I. I designed all the experiments. I conducted all the experiments except the ICP-AES measurements. I performed the data analysis and wrote the manuscript with input from the co-authors.

II. I designed the experiments with input from the co-authors. I conducted most of the experiments. I performed the data analysis and wrote the manuscript with input from the co-authors.

III. I designed all the experiments. I conducted all the experiments except the ICP-AES measurements. I performed the data analysis and wrote the manuscript with input from the co-authors.

IV. I participated in the design of the experiments. I conducted all the experiments except the actual operations of the scanning electron microscope. I performed the data analysis and wrote the manuscript with input from the co-authors.

V. I designed all the experiments. I conducted all the experiments except the XPS and ICP-AES measurements. I performed the data analysis and wrote the manuscript with input from the co-authors.

Contents

Abbreviations

AC	Alternating-current
CC	Constant-current
CCCV	Constant-current followed by constant-voltage
CMC	Sodium carboxymethyl cellulose
CV	Constant-voltage
DC	Direct-current
DMC	Dimethyl carbonate
EC	Ethylene carbonate
EIS	Electrochemical impedance spectroscopy
FEC	Fluoroethylene carbonate
ICI	Intermittent current interruption
ICP-AES	Inductively coupled plasma atomic emission spectroscopy
LFP	Lithium iron phosphate
LiTDI	Lithium 4,5-dicyano-2-(trifluoromethyl)imidazolide
LME	Lithium-metal electrode
NCA	Lithium nickel cobalt aluminum oxide
NMC	Lithium nickel manganese cobalt oxide
PE	Polyethylene
PP	Polypropylene
SEI	Solid electrolyte interphase
SEM	Scanning electron microscopy
SIMS	Secondary ion mass spectrometry
SOC	State of charge
VC	Vinylene carbonate
XPS	X-ray photoelectron spectroscopy
XRD	X-ray diffraction

1. Introduction

1.1 Lithium-based batteries and the negative electrodes

Ever since the discovery of lithium in Sweden in the early 1800s, the first metal in the periodic table has been destined to change human history. Lithium has a very high theoretic capacity of 3861 mAh g^{-1} and a very low standard potential of -3.04 V (vs. the standard hydrogen electrode).[1] The attempts to harness the power of lithium in electrochemical energy storage devices started after the determination of its electrochemical potential in 1913.[2] At the early stages, scientists and engineers tried to use lithium metal directly as the negative electrode in lithium-based batteries. However, the development of rechargeable batteries using lithium-metal electrodes (LMEs) did not really succeed. This was due to the high electrochemical reactivity of lithium metal with respect to liquid electrolytes and the poor lithium deposition and stripping performances, which made the batteries very difficult and also unsafe to be repeatedly charged and discharged. Later, instead of directly using lithium metal, the intercalation concept was adopted, and, together with the development of intercalation materials as the hosts for Li^+ as well as successful identification of suitable electrolytes, the first-generation lithium-ion battery was commercialized by SONY in 1990.[2][3]

Since then, more than 30 years have passed. With that design as the foundation, current lithium-ion batteries consist of transition metal oxides (e.g., $Li(Ni_xMn_yCo_z)O_2$ (NMC), $Li(Ni_xCo_yAl_z)O_2$ (NCA), $LiFePO_4$ (LFP)) as the positive electrode material, ca. 1.0 M $LiPF_6$ in ethylene carbonate (EC) based solvent mixtures as the base-line electrolyte, and mainly graphite as the negative electrode material. Polypropylene (PP) and/or polyethylene (PE) based membranes are used as the separator to prevent direct contact between the negative and positive electrodes. During charge, the transition metals are oxidized with lithium leaving the structure of the transition metal oxide in the form of Li^+ into the electrolyte and electrons leaving the positive electrode via the outer circuit. At the same time, graphite is reduced by the electrons entering the negative electrode with a same number of Li^+ in the electrolyte entering the graphite structure. The general process of lithium entering and leaving an electrode material is called lithiation and delithiation, respectively. During discharge, the flows described above are reversed. The positive electrode material is instead lithiated and the negative electrode material is delithiated. A schematic illustration is shown in **Figure 1.1**.

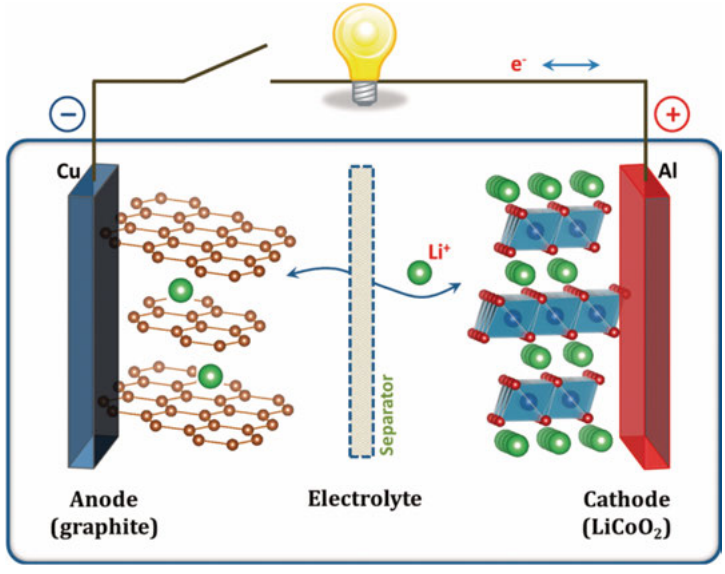

Figure 1.1. Schematic illustration of the first lithium-ion battery cell. Although $LiCoO_2$ is actually not commonly used as the positive electrode material anymore, the intercalation concept is "inherited". During charge and discharge, the electrons, e^-, and Li^+ move to the left and right, respectively. Reprinted with permission from [3]. Copyright (2013) American Chemical Society.

With higher and higher demands for better lithium-based batteries that have longer cycling lifetimes and/or higher energy densities, improving the current graphite based negative electrodes and/or enabling the use of new negative electrodes becomes crucial.

The negative electrode is generally considered to play an important role in the degradation of lithium-based batteries. In a battery cell, the negative electrode is operated at rather low potentials close to the Li^+/Li standard potential. Thus, many irreversible side reactions can occur. A major side reaction involves reductive decomposition of the electrolyte to form a solid electrolyte interphase (SEI) layer, which is composed of relatively insoluble decomposition products.[4][5] The formation of such a SEI layer on the surface of the graphite electrode is actually one of the key steps behind the realization of lithium-ion batteries since the SEI layer can (kinetically) hinder further electrolyte decomposition and hence allow proper cycling of the batteries.[2] However, the SEI layer is not completely electrochemically, chemically and mechanically stable. This means that continuous SEI layer (re)formation/maintenance can take place, e.g., due to the cracking of the layer and/or the negative electrode material itself as a result of volume changes during the cycling. This will cause continual consumption of charge and Li^+ and thus gradually decrease the available capacity of the battery cells.[5]–[9] In addition to the volume expansion and SEI formation effects, the rising sustainability awareness within the battery sector has also generated considerable research interest in

multi-level degradation mechanisms that limit the cell cycle life performances.[10]–[19] Among them, lithium plating (i.e., instead of entering the negative electrode material, Li^+ is in this case reduced to elemental Li on the electrode surface) is another important issue associated with the negative electrode. This can happen when, for several reasons, the (local) potential of the negative electrode drops to a potential where the deposition of lithium can start under the employed conditions.

Among new negative electrode materials, silicon is a promising candidate with a very high specific capacity compared with graphite, a decently low working potential, high abundance and low cost.[20]–[22] In contrast to intercalation materials like graphite, silicon forms alloys with lithium during the lithiation (i.e., an alloy-forming material), which leads to a considerable volume expansion.[23] The huge volume change during lithiation and delithiation is usually considered to be the major problem that limits the application of silicon based electrodes, since it can lead to silicon particle pulverization due to high internal stress. This inevitably yields unstable SEI layers and can potentially result in a loss of electronic contact with the particles.[24]–[27] Currently, the well-established strategy to circumvent these issues is to decrease the size of the employed silicon particles to the nanometer scale (particularly smaller than 150 nm).[25]–[30] Although silicon electrodes based on silicon nanoparticles usually perform much better than those based on silicon microparticles, the performances are still quite limited and far from competitive with respect to practical applications.

Different from intercalation and alloy-forming materials, the utilization of LMEs involves lithium deposition and stripping as mentioned above. Despite the failures in the early years, the research community has never stopped trying to find ways to properly control and stabilize the cycling of LMEs since lithium-metal batteries can have much higher gravimetric and volumetric energy densities than contemporary lithium-ion batteries.[31] However, in order to fully exploit the merits of lithium metal in lithium-metal batteries, a configuration with zero lithium metal excess at the negative electrode should be adopted (i.e., by directly depositing (and then stripping) lithium on (from) the current collector). Since such a configuration is constructed essentially by removing the negative electrode material coating in lithium-ion batteries, the corresponding lithium-metal batteries are generally called “anode-material-free” (or “anode-free”) lithium-metal batteries. Although anode-free lithium-metal batteries can achieve even higher (volumetric, especially) energy densities, without the “ capacity buffer” provided by the excess lithium as present in regular lithium-metal batteries, their cycle life performances are still extremely limited.[31][32]

In this thesis, the studies span from conventional graphite electrodes, silicon electrodes based on silicon nanoparticles, LMEs to the anode-free configuration with a particular focus on two scientific problems, i.e., diffusion-controlled lithium trapping and inhomogeneous lithium deposition.

1.2 Diffusion-controlled lithium trapping

Paper I-III focus on diffusion-controlled trapping of lithium (i.e., coupled Li^+ and e^- or elemental Li) in negative electrodes based on graphite or silicon nanoparticles, respectively.

1.2.1 The model and mechanism

In order to improve the cycling lifetimes of current lithium-ion batteries or enable new lithium-ion batteries with higher energy densities using new materials, a better and more complete understanding of all phenomena that limit the cell performances is essential. For negative electrodes based on alloy-forming materials such as silicon, aluminum and tin, it has, recently been shown that capacity losses can result from diffusion-controlled trapping of elemental Li in the materials as this gradually decreases the available "space" that can be used for lithiation during cycling.[33]–[41] Such a lithium trapping effect was, in fact, proposed to be the main cause of the capacity losses seen during the cycling of silicon nanoparticle based electrodes in half cells containing LMEs as the counter electrodes.[33]–[35]

The diffusion-controlled lithium trapping effect is based on the two-way diffusion trapping model introduced by Rehnlund et al., and a schematic illustration of the underlying mechanism is shown in **Figure 1.2**.[33]–[35] Before discussing this trapping model, it is very important to note that the real situations and conditions should be much more complicated than what can be seen in **Figure 1.2**. The schematic illustration only provides a very simplified picture for the purpose of describing the concept. During constant-current (CC) lithiation, lithium diffuses into the electrode and a concentration gradient is formed with a higher concentration of lithium close to the electrode surface (i.e., the electrolyte side). Then, when the following CC delithiation starts, the lithium concentration at the electrode surface starts to decrease, resulting in a concentration profile with an intermediate region possessing a higher lithium concentration than that both at the electrode surface and in the inner region of the electrode (i.e., closer to the current collector). Such a concentration profile leads to lithium redistribution within the electrode via diffusion (i.e., lithium moving along the concentration gradient(s)) also during the CC delithiation step. As a result, a small portion of the inserted lithium which has diffused too deep into the electrode to be extracted within the time domain of the CC delithiation step becomes trapped in the electrode (see **Figure 1.2** top row). Due to the presence of the trapped lithium, the subsequent lithiation becomes hindered/limited, which is reflected in a decreased lithiation capacity (i.e., a capacity loss) and/or a shift in the lithiation potential. In addition, another small portion of lithium can again be trapped on this cycle (see **Figure 1.2** middle row). After certain number of cycles, the accumulation of the trapped lithium can eventually lead to the practical failure of the electrode as there is no longer

any electrochemically meaningful free space in the electrode for additional lithium (see **Figure 1.2** bottom row).

The influence of the diffusion-controlled lithium trapping effect depends strongly on the time domains of the (typically, CC based) lithiation and delithiation steps, the lithium diffusion rates and diffusion path lengths, as well as the lithium concentration profile (developed) in the electrode.[35] In this regard, it has been demonstrated that a constant-voltage (CV) delithiation step, included after CC delithiation, can be used to extract some of the trapped lithium from a silicon nanoparticle based electrode by prolonging the duration of the delithiation process.[34] This can decrease the influence of the trapping effect and hence extend the electrode cycling lifetime.

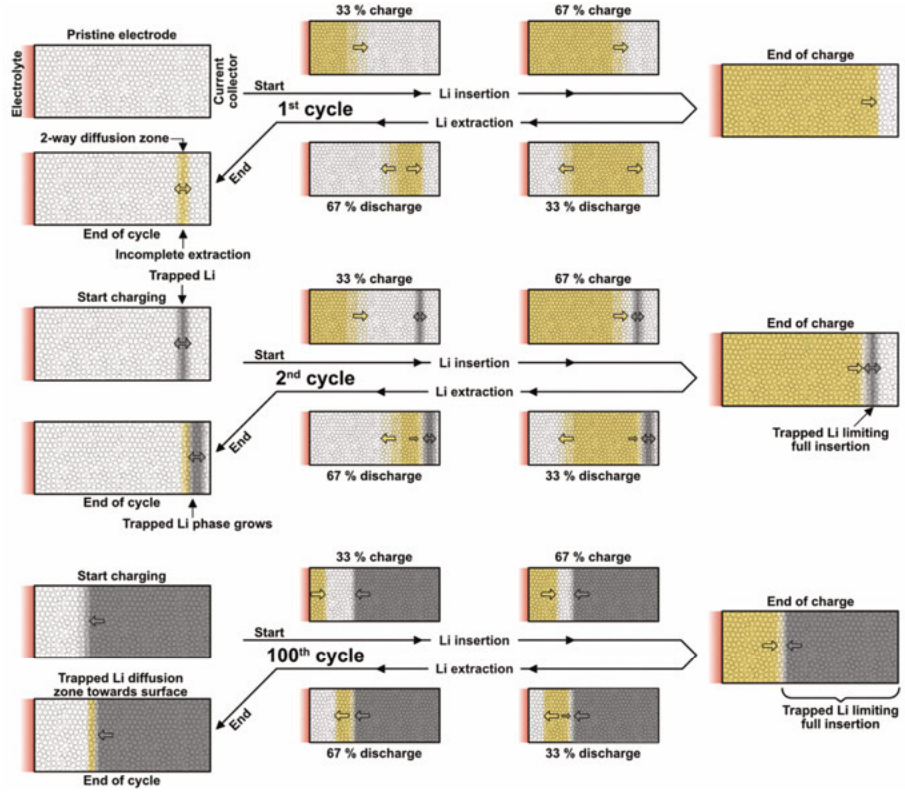

Figure 1.2. Schematic illustration of the mechanism behind the diffusion-controlled lithium trapping effect. Reprinted from the open-access review by Rehnlund et al.[35] Note that the figure only provides a very simplified picture and hence cannot fully represent real situations and conditions.

1.2.2 In graphite electrodes

As describe above, the diffusion-controlled lithium trapping effect stems from incomplete delithiation of the negative electrode due to lithium concentration gradients. Thus, it is reasonable to assume that diffusion-controlled trapping of lithium (i.e., coupled Li^+ and e^-) should also be seen for negative electrodes based on intercalation materials, such as graphite, given that inhomogeneous lithiation and delithiation issues are widely found for graphite electrodes.[42]–[46] In fact, there are published experimental results suggesting the presence of lithium trapping in graphite electrodes, even though the authors were actually focusing on other topics.[46]–[52] Two examples are described below.

By using secondary ion mass spectrometry (SIMS), Li et al.[47] found that some lithium was located deep inside a delithiated graphite electrode after being cycled in a full cell for 1500 cycles. The presence of trapped lithium was further supported by the fact that, in the subsequent half-cell experiments, the first phase transition plateau that should be seen at 20-35 mAh g^{-1} was absent, causing the voltage to drop directly to the LiC_{12} phase transition plateau during the lithiation of the cycled graphite electrode (see **Figure 1.3**). In another study where Finegan et al.[52] used high-speed depth-profiling synchrotron X-ray diffraction (XRD) to study the cycling of graphite electrodes in operando, two-way lithium diffusion was observed during the delithiation. As can be seen in **Figure 1.4**, the amounts of the LiC_{12} species in the deeper regions (i.e., closer to the copper current collector) were found to increase during the delithiation, without a corresponding decrease in the amounts of the LiC_6 species, while the amounts of the two species in the more surface-close regions were decreasing. Furthermore, residual lithiated graphite species were found at the end of the delithiation when the full cell was discharged to 2.8 V.

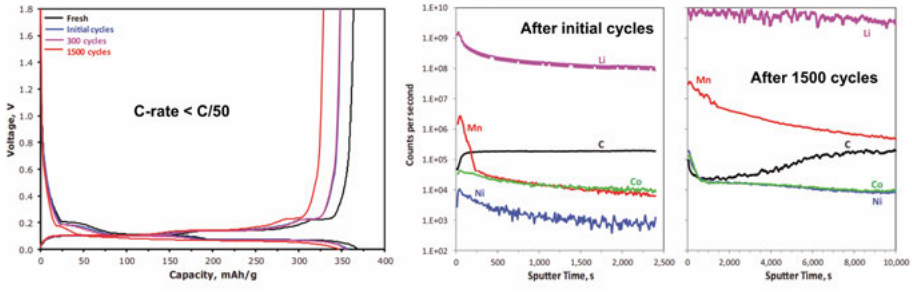

Figure 1.3. Experimental results from a previous study by Li et al.[47] showing (left) the lithiation and delithiation curves seen for the fresh graphite electrode and the harvested ones after being cycled in full cells for different numbers of cycles, and (right) SIMS sputter depth profiles of the graphite electrodes after initial and 1500 cycles, respectively. Note that the sputter time scales on the x-axes are different. Adapted and reprinted with permission from [47]. Copyright (2013) IOP Publishing.

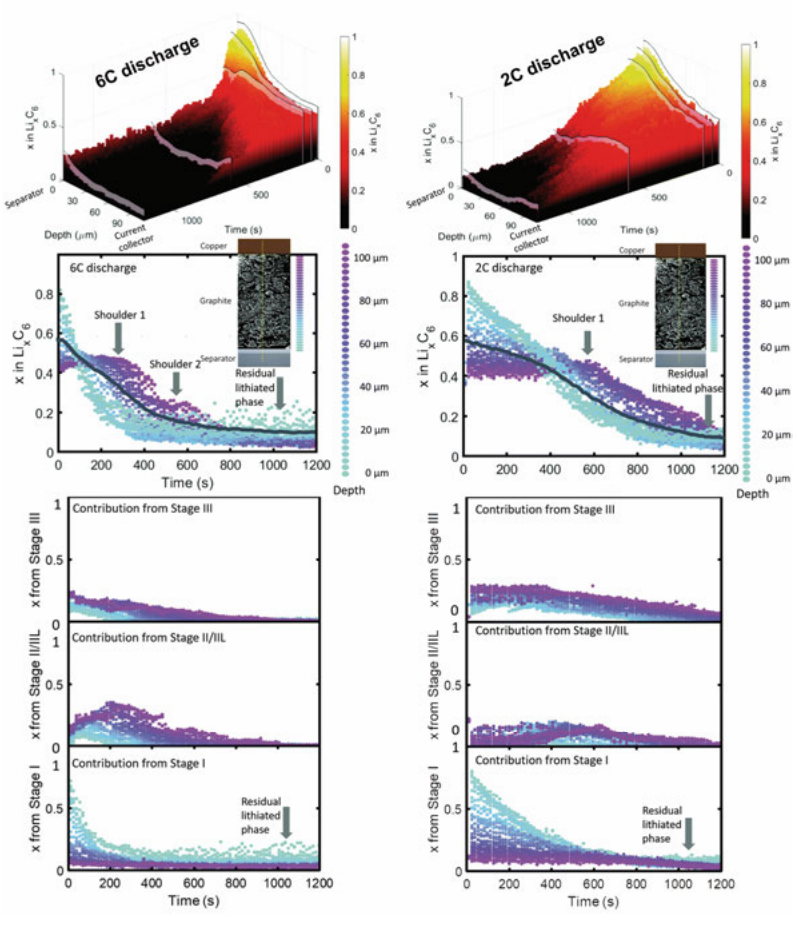

Figure 1.4. Experimental results from a study by Finegan et al.[52] showing the time- and depth-resolved (de)lithiation degrees of the graphite electrodes and contributions from different lithiated graphite species during the discharge of the full cells cycled at different C-rates (i.e., 3C and 6C, respectively). Stage III, II/IIL and I corresponded to the LiC_{30}, LiC_{12}/LiC_{18} and LiC_6 species, respectively. Adapted and reprinted with permission from [52]. Copyright (2020) Royal Society of Chemistry.

It is crucial to investigate the presence of a diffusion-controlled lithium trapping effect in graphite electrodes since its impact on contemporary lithium-ion batteries can be multiple and significant. As the graphite electrodes are gradually filled up with trapped lithium due to the trapping effect, their lithiation will become more and more hindered with increasing overpotentials. This can greatly increase the risk of lithium plating[10]–[14] and hence lead to not only further capacity losses of the cells but also safety hazards. Furthermore, as a result of the lithium trapping, the positive electrodes will be cycled at higher delithiated states. This may facilitate irreversible phase changes, structure instabilities and parasitic reactions involving the electrodes.[10]–[12][16] Therefore, identifying the trapping effect and then developing strategies to mitigate it

early on during cycling should be very important for the realization of battery cells with considerably improved cycle life performances. This is particularly essential in conjunction with high-rate cycling as the latter should increase the influence of the trapping effect and consequently also the abovementioned associated issues.[14]–[18] In **Paper I**, the presence and cause of a diffusion-controlled lithium trapping effect in graphite electrodes were studied. Its impact on the full-cell high-rate cycling performances was further demonstrated in **Paper II**. At the same time, a mitigation approach was proposed and discussed.

1.2.3 In silicon nanoparticle based electrodes

Although the model of diffusion-controlled lithium trapping was originally developed largely on the basis of silicon nanoparticle based electrodes as mentioned in Section 1.2.1,[33]–[35] a deep and comprehensive understanding of the trapping effect seen for such electrodes has still been lacking. Being able to identify and specify, e.g., the role of the silicon nanoparticle size in the trapping model should be important, since the performances of silicon nanoparticle based electrodes are of broad interest and particle size related topics have received a lot of attention.[24][27][53]–[57]

As mentioned in Section 1.2.1, the influence of the trapping effect depends on the lithium diffusion path lengths.[35] This means that it should practically depend on the size of the silicon nanoparticles used in a silicon electrode. According to the trapping model, it can be expected that a smaller particle size should result in lower capacity losses since the lithium diffusion length in the particles is shorter.[33][35] However, it should be noted that the time required for lithium to diffuse to the center of silicon nanoparticles with diameters of, e.g., 100 and 50 nm should be only about 12 and 3 seconds, respectively, assuming a solid-state diffusion coefficient of 10^{-12} cm^2 s^{-1}.[33][58] In addition, it is very unlikely that all the silicon nanoparticles in the electrode are in direct contact with the electrolyte. These indicate that the diffusion-controlled trapping effect must be discussed on the electrode level, most likely involving inter-particle solid-sate diffusion of lithium and various lithium diffusion paths, rather than on the individual nanoparticle level. It is thus not immediately clear how the nanoparticle size will affect the influence of the trapping effect seen for silicon nanoparticle based electrodes. In **Paper III**, this is explicitly investigated and discussed.

1.3 Lithium deposition

Paper IV and **V** concern lithium deposition on LMEs and copper current collectors for regular and anode-free lithium-metal batteries, respectively.

1.3.1 The electrochemical nucleation/deposition theory

Electrodeposition theory and practice have been developed and widely used for metal electrodeposition in other fields than lithium-based batteries.[59][60] According to the electrochemical nucleation/deposition theory, the critical free energy for the nucleation, ΔG_c, and the critical radius of the nuclei, r_c, can be calculated as

$$\Delta G_c = \frac{16\pi M^2 \gamma^3}{3\rho^2 n^2 F^2 \eta^2}$$

$$r_c = \frac{-2M\gamma}{nF\rho\eta}$$

where M is the molecular weight, γ is the molar surface free energy, ρ is the density of the electrodeposit, n is the number of electrons involved in the electrodeposition reaction, F is the Faraday constant, and η is the overpotential. The critical free energy represents the energy barrier that needs to be overcome for the nucleation to take place and hence affects the nucleation rate, whereas the critical radius defines the minimum size of the nuclei needed for the nuclei to "survive" and then grow. Sufficiently small clusters are hence not stable and tend to undergo "dissolution". For the electrodeposition of a certain metal, the major variables that can be practically controlled are the surface free energy, γ, and the overpotential, η. Since γ may vary with, e.g., temperature, it should be possible to change ΔG_c and hence adjust the nucleation rate by tuning the electrodeposition temperature.[61]

According to the equations above, the use of a higher η will lead to a decrease in both ΔG_c and r_c. Hence, the nucleation process should then be facilitated given that more clusters can reach the critical radius needed to form stable nuclei with a lower energy barrier. A higher η will therefore lead to the formation of a greater number of small(er) nuclei on the electrode/substrate surface, while a low η will only give rise to a limited number of large(r) nuclei preferentially at the most (electrochemically) favorable sites on the surface. In order to obtain a uniform two-dimensional deposit, homogeneous and instantaneous nucleation during the initial nucleation stage is highly preferred. In this context, instantaneous (in contrast to progressive) nucleation refers to a nucleation process in which the nuclei are formed only at the beginning of the electrodeposition and there is hence no further nuclei formation throughout the rest of the process.

Here, it is, however, important to note that the application of the nucleation theory is usually limited to qualitative descriptions due to the fact that some of the assumptions it is based on (e.g., that the properties of the clusters are the same as those of the corresponding bulk materials) do not necessarily reflect the reality.[59][60]

The nucleation theory was qualitatively exploited in **Paper V** for the deposition of lithium on copper current collectors, while its concept likewise was found to be applicable to the stripping of LMEs in **Paper IV**.

1.3.2 On lithium-metal electrodes

The major issue that still hinders the practical application of LMEs is the inability to properly control the deposition of lithium. Ideally, uniform (not just homogeneous) two-dimensional lithium deposition is desired. However, inhomogeneous three-dimensional lithium deposition is usually obtained. This is particularly true in conventional electrolytes consisting of 1.0 M $LiPF_6$ in EC based solvent mixtures.[62]–[65] By nature, when one applies a constant current, the electrochemical reaction with "smallest hinderance" will take place first in an electrochemical cell. This also applies to CC cycling of LMEs. An operando visual observation made by Wood et al.[63] can be used as a schematic support to describe the problems during the CC cycling of LMEs. As can be seen in **Figure 1.5**b, lithium deposition only takes place at certain spots/regions on the electrode surface, resulting in the formation of mossy lithium with other regions remaining almost unaffected. Similarly, if one starts the cycling with lithium stripping, it will also take place inhomogenously, which has been observed in other studies[66]–[69] and was discussed in **Paper IV**. During the subsequent stripping step, the mossy lithium starts to shrink due to the dissolution of the generated Li^+ into the electrolyte (see **Figure 1.5**c and d). Because of inhomogeneous stripping, "dead lithium" which is lithium that has "electrochemically detached" from the LME is formed. Since the dead lithium is electrochemically inactive, Li^+ then need to be generated and extracted from somewhere else on the LME surface in order to continue the CC stripping step. As a result, pits are formed in other regions on the LME surface (see the yellow circles in **Figure 1.5**e and f). This pit formation gives rise to a voltage increase (i.e., higher overpotential) since pitting is electrochemically less favorable and hence requires a larger electrochemical driving force (see **Figure 1.5**d and e). Thus, after a complete cycle, the LME has dead lithium and pits on its surface. Eventually, after repeated cycling, the LME will become more and more porous with an increasing impedance due to the accumulation of dead lithium and further formation of pits, resulting in a short cycling lifetime.[70]

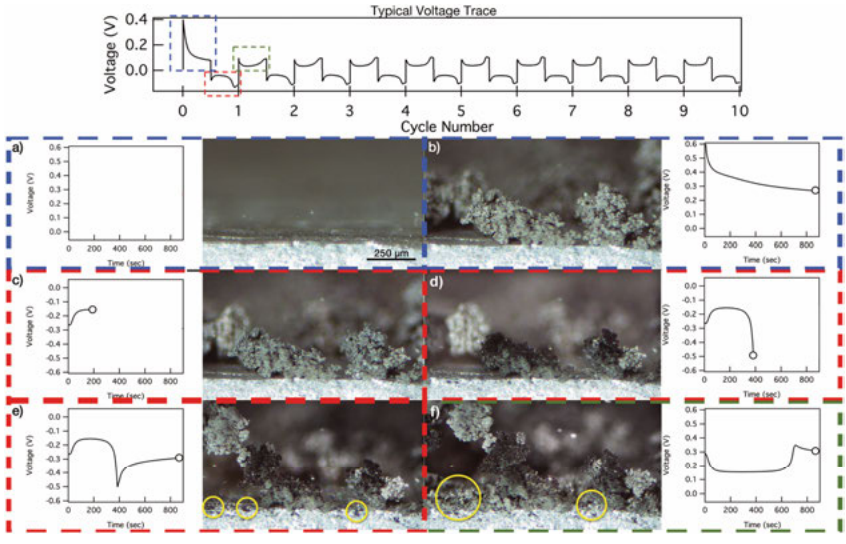

Figure 1.5. Operando visual observation of CC lithium deposition and stripping during the first 1.5 cycles in a two-electrode lithium symmetric cell. The colors of the frames indicate different stages of the cycling by order, while the yellow circles highlight the formation of pits on the LME surface. Note that the voltage trace was presented in an inverted way. If the two LMEs in the cell can be denoted as LME1 and LME2, the voltages were actually recorded as the potential differences between LME1 and LME2, despite the fact that it was LME2 that was being observed optically. Reprinted from the open-access article by Wood et al.[63]

To circumvent the problems described above, many material- and chemistry-based strategies involving, e.g., conductive porous hosts or composite matrixes, artificial SEI layers and modified electrolytes have been proposed to stabilize LMEs.[66][71]–[73] Conductive porous hosts or composite matrixes can, e.g., decrease the practical current density, provide a more homogeneous substrate for lithium deposition and act as a caged entrapment to accommodate lithium and thus limit overall volume change during the cycling.[74][75] An artificial SEI layer, obtained by, e.g., coating a thin and homogeneous protective layer on the LME surface, may facilitate more homogeneous lithium deposition as such a layer can reduce the "active sites" problem and/or has a higher mechanical strength to withstand the mechanical stress induced by volume change during the cycling.[76][77] Modifications of the electrolyte by, e.g., adding additives and/or changing the salts and/or solvents aim at forming a more stable SEI layer with better electron insulating and lithium-ion conducting properties via (preferential) decompositions of certain components.[78][79]

However, there are not so many studies addressing the stability problems of LMEs from a more fundamental electrochemical aspect by, e.g., attempting to electrochemically control the nucleation and subsequent growth of lithium. Recently, Rehnlund et al., demonstrated that two-dimensional lithium deposition could be attained by decreasing the concentration of the $LiPF_6$ salt in the

electrolyte from 1.0 M to 0.02 M and applying a potentiostatic nucleation pulse with a duration of 10 ms prior to initial deposition on the first cycle.[67] This combination allowed a high overpotential to be achieved, which led to a large number of homogeneously distributed nuclei formed on the LME surface during the initial nucleation stage. The nuclei then grew under normal CC (or pulsed-current) conditions. However, this nucleation approach was not that effective in conventional 1.0 M $LiPF_6$ electrolytes since the LME should then function as an almost ideally nonpolarizable electrode (i.e., a very high current is required to shift its potential). Therefore, finding a potential alternative approach that is compatible with conventional 1.0 M $LiPF_6$ electrolytes should be very beneficial to the development of lithium-metal batteries. This possibility was explored in **Paper IV**.

1.3.3 On copper current collectors

The deposition of lithium on a copper current collector differs from that on a LME with additional complexities.[80] Due to the presence of a native oxide/hydroxide layer on the copper surface, conversion reactions yielding a surface layer composed of Cu nanoparticles and Li_2O will occur in the early stage of the (first) reduction step. This and the formation of a SEI layer due to the electrochemical reduction of the electrolyte (at lower potentials than the conversion reactions) take place prior to the onset of lithium deposition on copper. Moreover, according to the Nernst equation, the lithium deposition potential should depend on the lithium activity at the copper surface. The latter activity should initially be much lower than unity and gradually increase as the deposition proceeds. This means that, thermodynamically, the lithium deposition potential will keep decreasing until the copper surface has been coated with a layer of lithium.

In spite of the complexities, the problems regarding lithium deposition (and stripping) are essentially the same for LMEs and copper current collectors. Many material- and chemistry-based strategies have also been proposed to improve the lithium deposition on copper current collectors in anode-free cells.[32][81]–[83] Among them, the development of new electrolyte formulations, affecting the Li^+ solvation structure and/or the compositions and morphologies of the SEI layer, constitutes the major chemistry-related approach.[84]–[91] Other material-related approaches involve (i) modifications of the copper current collectors by synthesizing three-dimensional structures to lower the local current densities and encapsulate the deposited lithium, (ii) designs of artificial SEI layers that are more stable during the lithium deposition, and/or (iii) coating so-called “lithiophilic” material(s) on the copper surface to facilitate the nucleation and deposition of lithium.[92]–[101]

However, in addition to the well-known complexities mentioned above, there is another effect, i.e., diffusion of lithium into copper, that may influence the lithium deposition but has not been explicitly studied and discussed. It has

been shown that the deposition of lithium on copper results in lithium diffusing into the copper.[102]–[105] In the study by Rehnlund et al., a layer of lithium with a thickness of about 25 nm was deposited on copper nanorods in an attempt to manufacture a three-dimensional lithium nanoelectrode.[102] The deposited lithium was, however, found to diffuse into the nanorods, resulting in a rapid capacity loss of the electrode. This result shows that the effect of the diffusion can be readily seen after depositing a small amount of lithium (as would be the case during the lithium nucleation stage). Using operando neutron depth profiling to track the spatial distribution of lithium during lithium deposition and stripping on copper, Lv et al. found out that some lithium was actually taken up by the copper substrates, most likely via the grain boundaries, during the deposition (see **Figure 1.6**).[103] This finding further indicates that the diffusion of lithium into copper will take place simultaneously while lithium is being deposited on copper. The diffusion phenomenon is in fact not surprising as a solid solution with up to 13-14 atom% Li can form according to the Cu-Li phase diagram.[106] Furthermore, the fact that lithium can enter and move through copper swiftly enough has actually been exploited to develop protective copper coatings (with a thickness up to 100 nm) on silicon nanomaterials for lithium-ion batteries.[107]–[109]

The lithium diffusion phenomenon described above can have a negative impact on the deposition since it may significantly affect the stability of lithium clusters (i.e., nuclei "embryos") on the copper surface during the nucleation step. In **Paper V**, the influence of such diffusion on the nucleation/deposition of lithium on copper current collectors was explicitly investigated.

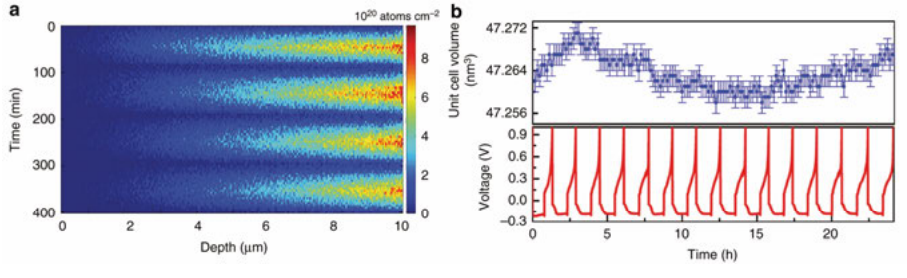

Figure 1.6. (a) The operando neutron depth profiling experiment, showing the lithium uptake in a copper current collector during the deposition and stripping of lithium. Note that the depth on the x-axis actually refers to the thickness of the copper current collector (i.e., the current collector surface was situated at a depth of 10 μm). (b) The variation of the copper lattice parameter derived from the operando XRD experiment, demonstrating no correlation with the cycling and hence the lithium uptake. Reprinted from the open-access article by Lv et al.[103]

2. Scope of the thesis

In this thesis, two scientific problems that are related to negative electrodes and/or negative electrode materials for lithium-based batteries were studied. The first one involves the diffusion-controlled lithium trapping effect. The inability to completely delithiate negative electrode materials can lead to their degradation and capacity losses upon cycling, which eventually shortens the cycling lifetimes of the battery cells. The second problem concerns inhomogeneous deposition (and stripping) of lithium, which strongly hinders the applications of regular and anode-free lithium-metal batteries.

In order to have lithium-based batteries with longer cycling lifetimes and/or higher energy densities, it is essential to address these two problems, preferably based on improved scientific understandings.

In **Paper I**, the aim was to explicitly investigate and demonstrate the presence of a diffusion-controlled lithium trapping effect in graphite electrodes and to develop an electrochemical approach to decrease its influence on the electrochemical performances of the electrodes.

In **Paper II**, which was based on the findings presented in **Paper I**, the aim was to study the impact of the diffusion-controlled trapping effect on the high-rate cycling performances of NMC811/graphite full cells and to obtain an improved understanding for facilitating the realization of stable and prolonged cell cycle life under high-rate cycling.

In **Paper III**, the aim was to study the influence of the particle size on diffusion-controlled lithium trapping in silicon nanoparticle based electrodes and to form an improved understanding of the trapping effect seen for such electrodes.

In **Paper IV**, the aim was to establish an electrochemical strategy for improving lithium deposition on LMEs in conventional 1.0 M $LiPF_6$ electrolyte to stabilize the cycling performances, by electrochemically controlling the lithium nucleation process.

In **Paper V**, the aim was to investigate the influence of lithium diffusion into copper current collectors on lithium nucleation/deposition and to explore the possibility of attaining homogeneous lithium deposition on the current collectors by improving the nucleation of lithium.

3. Materials and methods

3.1 Materials and cell assemblies

The key materials and the configuration of the cells used in each study are described here roughly. The readers are referred to the corresponding papers for more details.

In **Paper I**, the presence and cause of a diffusion-controlled lithium trapping effect in graphite electrodes were investigated. Experiments were carried out using two-electrode graphite/Li CR2025 coin cells (see **Figure 3.1**a). The in-house fabricated graphite electrodes (13 mm in diameter) contained 93% SLP30 graphite, 5% sodium carboxymethyl cellulose (CMC) and 2% C65 conductive carbon black, by weight, and the graphite mass loading was around 2.80 mg cm^{-2}. Commercial lithium disks (450 μm in thickness and 15 mm in diameter) were used as the lithium counter electrodes. The two electrodes were separated by a Celgard 2400 separator soaked with LP40 electrolyte (i.e., 1 M $LiPF_6$ in EC: diethyl carbonate (DEC) = 1:1 (v/v)).

In **Paper II**, the influence of the diffusion-controlled lithium trapping in graphite electrodes on the cycling performance of NMC811/graphite full cells was studied. Experiments were carried out using two-electrode CR2025 coin cells (see **Figure 3.1**b). Commercial NMC811 and graphite electrodes (both 13 mm in diameter) were used, and they were separated by a Celgard 2400 separator soaked with LP40 electrolyte.

In **Paper III**, diffusion-controlled lithium trapping seen for silicon electrodes based on silicon nanoparticles of three different sizes (i.e., 100, 50-80 and ≤50 nm) was studied and the cycling performances were compared. The silicon electrodes were denoted as "SiNP100", "SiNP50-80" and "SiNP≤50", respectively. Experiments were carried out using two-electrode Si/Li CR2025 coin cells (see **Figure 3.1**a). The in-house fabricated silicon electrodes (17 μm in thickness and 13 mm in diameter) contained 70% silicon nanoparticles, 10% CMC and 20% C65 conductive carbon black, by weight, and the silicon mass loadings were around 0.90, 0.75 and 0.61 mg cm^{-2} for the SiNP100, SiNP50-80 and SiNP≤50 electrodes, respectively. Commercial lithium disks (450 μm in thickness and 15 mm in diameter) were used as the lithium counter electrodes. The two electrodes were separated by two Solupor 3P07A separators soaked with electrolyte composed of 0.6 M lithium 4,5-dicyano-2-(trifluoromethyl)imidazolide (LiTDI) in dimethyl carbonate (DMC): EC: fluoroethylene carbonate (FEC): vinylene carbonate (VC) = 2:1:0.1:0.02 (v/v/v/v).

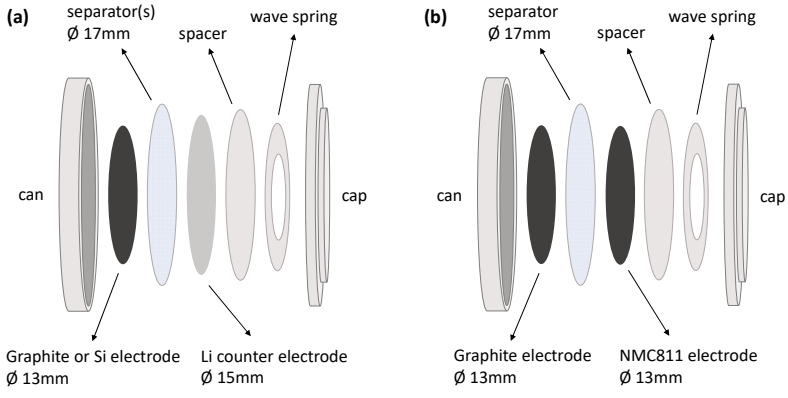

Figure 3.1. Illustrations of the two-electrode coin cells used in (a) **Paper I** and **III** and (b) **Paper II**.

In **Paper IV**, the lithium stripping and deposition behaviors of LMEs were studied. Experiments were carried out using three-electrode Li/Li symmetric pouch cells (see **Figure 3.2**). The LMEs used as the working and counter electrodes were prepared by simply punching lithium foil (125 μm in thickness) into disks with a diameter of 14 mm, while a rectangular piece of lithium foil was used as the reference electrode. The electrodes were separated by two Celgard 2400 separators soaked with LP40 electrolyte.

In **Paper V**, the deposition of lithium on copper current collectors was studied. Experiments were carried out using three-electrode Li/Cu pouch cells in which two LMEs were employed as the counter and reference electrode, respectively, whereas a "pure" copper substrate or a "prelithiated" copper substrate was used as the working electrode (see **Figure 3.3**). The electrodes were separated by two Solupor 3P07A separators soaked with LP40 or "low-LP40" electrolyte (see below). The LMEs were prepared by simply punching lithium foil (130 μm in thickness) into disks with a diameter of 10 mm, while the pure copper substrates (13 mm in diameter) were punched out from battery-grade copper foil (10 μm in thickness). The prelithiated copper substrates were prepared by keeping the copper disks in tight contact with a piece of lithium foil at 70°C for 30 days under vacuum. The composition of the low-LP40 electrolyte was 0.020 M $LiPF_6$ and 1.0 M tetrabutylammonium hexafluorophosphate ($TBAPF_6$) in EC:DEC = 1:1 (v/v).

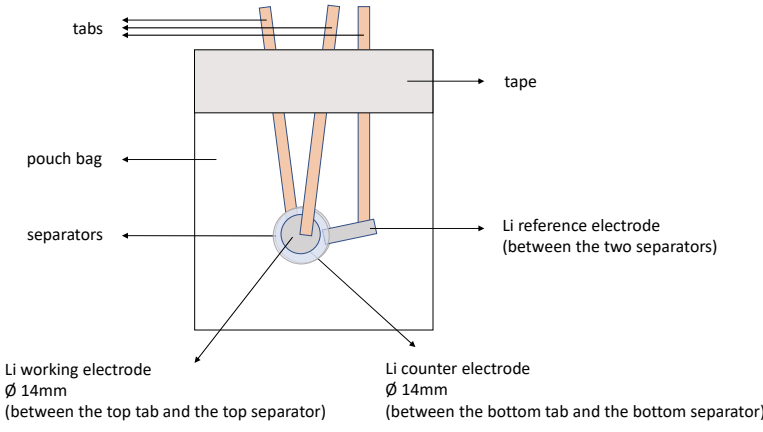

Figure 3.2. An illustration of the three-electrode cells used in **Paper IV**.

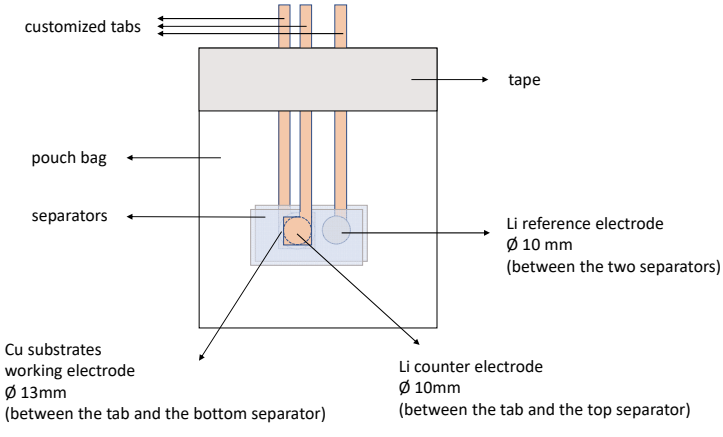

Figure 3.3. An illustration of the three-electrode cells used in **Paper V**.

3.2 Electrochemical techniques

3.2.1 Chronopotentiometry and chronoamperometry

Chronopotentiometry is a method in which a constant current normally is applied while the potential of the working electrode in a three-electrode cell or the cell voltage of a two-electrode cell is measured. By using chronopotentiometry, the electrochemical system is requested to conduct electrochemical reactions/processes at certain rates in order to support/withstand the constant current. Once the system no longer can support/withstand the constant current, for several reasons, the potential or cell voltage will change to provide a greater driving force and/or enable additional electrochemical reactions/processes. Typically, it is used with potential or cell voltage limits, so the current is applied until a certain potential or cell voltage value is reached. However, chronopotentiometry can also be used with time or capacity/charge limits. The potential or cell voltage variation can provide insights into the electrochemical behaviors of the electrode and electrode material(s) of interest. The most commonly conducted electrochemical experiment, i.e., CC cycling, in the field of lithium-based batteries is essentially a type of chronopotentiometry experiment. The term "C-rate" is usually used to describe the applied current, and a C-rate of, e.g., C/2 means that it will theoretically take two hours to fully (de)lithiate (or (dis)charge) the electrode (or cell) using such a current.

Chronoamperometry, on the other hand, is a method in which a constant potential is applied to the working electrode (e.g., in a three-electrode cell) while the current is measured. In the field of lithium-based batteries, where two-electrode cells are more commonly used, the concept can be adapted to apply a constant cell voltage. By using chronoamperometry, the electrochemical system is provided with a certain electrochemical drive force. All the electrochemical reactions/processes that can be triggered by such a driving force will take place and give rise to a current jointly. For several reasons, the electrochemical reactions/processes will gradually slow down and the current will decrease, eventually to nearly zero. Chronoamperometry is typically used with current or time limits, so the potential or cell voltage is applied until the current drops to certain value or for a certain time duration. Similar to the variation of the potential or cell voltage mentioned above, the variation of the current can likewise provide insights into the electrochemical behaviors of the electrode and electrode material(s).

In this thesis, chronopotentiometry and chronoamperometry were used with customized experimental designs in **Paper I-V** for different purposes. Chronoamperometry was particularly important in this thesis as the diffusion-controlled lithium trapping and lithium deposition studies relied heavily on the applications of CV and potentiostatic steps, respectively.

3.2.2 Intermittent current interruption method

The intermittent current interruption (ICI) method was developed by Lacey and Chien et al. based on the porous electrode model proposed by de Levie. The details as well as the validation of the method can be found in previous publications.[110]–[113] In short, every five minutes, a one-second pause is applied during CC cycling of a cell at a low C-rate. The internal resistances, R, and diffusion resistance coefficients, k, at various states of charge (SOCs) can be calculated from the intercepts and slopes, respectively, derived from linear fits to the plots of the voltage variation during each pause against the square root of the pause time, as

$$R = -\frac{\Delta E_{t=0}}{I}$$

$$k = -\frac{d\Delta E / d\sqrt{t}}{I}$$

where ΔE is the difference between the voltage during each pause of one second and that measured at the end of each five-minute long CC cycling "segment", t is the time passed after the end of each CC cycling segment of five minutes (i.e., since the current was switched off), and I is the current used for the CC cycling. The internal resistance, derived from the instant voltage drop that should be seen at the moment when the current is switched off, is the total resistance of the cell. Meanwhile, the diffusion resistance coefficient reflects the resistance associated with the (solid-state) lithium diffusion in the cell. The major advantage of the ICI method is that the variations in the resistance and diffusion condition/behavior can be tracked somewhat continuously during the lithiation and delithiation steps.

In this thesis, ICI experiments were conducted mainly to study diffusion-controlled lithium trapping in the graphite (**Paper I**, Section 4.1.3) and silicon nanoparticle based (**Paper III**, Section 4.3.1) electrodes.

3.2.3 Electrochemical impedance spectroscopy

In electrochemical impedance spectroscopy (EIS) experiments, electrochemical impedances are measured by applying alternating-current (AC) potentials with various frequencies to an electrochemical cell while recording the generated alternating currents. The impedances at different frequencies are then calculated by "dividing" the applied AC potentials by the generated alternating currents in analogy with Ohm's law for direct-current (DC) resistances. In contrast to a DC resistance, an AC impedance consists of a real and an imaginary part. The EIS experiment data is commonly presented in the form of Nyquist plot where the negative value of the imaginary part is plotted against

the real part. The frequency dependency of the AC impedance allows EIS to differentiate and describe impedances associated with different electrochemical processes on different time scales. It should be noted that the amplitude of the applied AC potentials should be low enough (usually 1 to 10 mV) so that the response of the electrochemical cell can be treated assuming a linear (or pseudo-linear) potential-current relation.[114] Another thing that needs to be considered is that the electrochemical cell should remain stable throughout the time span required to conduct the EIS measurements. This means that any drift in the DC potential(s) of the studied electrode(s) should be as small as possible, since it could affect the obtained data and hence the analyses (especially the fittings of the data).

In this thesis, EIS experiments were conducted to probe qualitative differences or changes in the electrochemical properties of the graphite electrodes (**Paper I**, Section 4.1.2) and LMEs (**Paper IV**, Section 4.4.2). In both these studies, a single EIS measurement took no longer than one minute.

3.3 Characterization techniques

3.3.1 Scanning electron microscopy

In scanning electron microscopy (SEM), a focused electron beam is used to scan the sample surface. The interactions between the incoming electrons and the sample can produce various types of electrons, X-rays and even light. The information they carry can be used to conduct various analyses.

In this thesis, SEM was mainly used to study the surface morphologies of the silicon nanoparticle based electrodes (**Paper III**, section 4.3.2) and LMEs (**Paper IV**, Section 4.4) as well as the morphologies of the lithium deposits obtained on the copper substrates (**Paper V**, Section 4.5).

3.3.2 Inductively coupled plasma atomic emission spectroscopy

Inductively coupled plasma atomic emission spectroscopy (ICP-AES) is a method that can be used to determine the amounts of different elements in samples. Solid samples (e.g., electrodes) must first be dissolved using proper processing methods, after which the obtained solutions (or suspensions) are filtered, if necessary, and then adequately diluted. The diluted solutions are then fed into the ICP-AES instrument where they will be vaporized and the contained elements will be atomized. The collisions of the atoms with the excited argon species lead to emissions of characteristic radiations which can be used to identify and also quantify, based on proper calibrations, the corresponding elements.

In this thesis, ICP-AES was mainly used to quantify the amounts of lithium in the delithiated cycled graphite (**Paper I**, Section 4.1.1) and silicon nanoparticle based **(Paper III**, Section 4.3.1) electrodes as well as in the prelithiated copper substrates (**Paper V**, Section 3.1 and 4.5.2).

4. Results and discussion

4.1 Diffusion-controlled lithium trapping in graphite electrodes

In this chapter, the results of a series of electrochemical half-cell experiments, designed to investigate the presence and cause of a diffusion-controlled lithium trapping effect in conventional graphite electrodes, are presented and discussed. In addition, an electrochemical approach is proposed to decrease the influence of such a trapping effect, and its effects are also discussed. Details can be found in **Paper I**.

4.1.1 Long-term capacity-limited cycling experiments

In order to investigate the presence of a diffusion-controlled lithium trapping effect and its potential influence on the electrochemical performances of graphite electrodes, long-term capacity-limited cycling experiments were conducted. In these experiments, the cells were cycled with a lithiation capacity limit of 170 mAh g^{-1} using two protocols: (i) capacity-limited CC cycling (i.e., standard CC cycling but with a capacity limit), and (ii) capacity-limited CC cycling with a CV step at 1 V following the delithiation to the cut-off voltage of 1 V on every fifth cycle from the 21st cycle. The latter is denoted as capacity-limited CCCV cycling.

As can be seen from the CC cycling curves presented in **Figure 4.1**a and b, the voltage drop towards the end of the lithiation became larger and larger when comparing the 126th, 351st and 516th lithiation curves. This implies that the insertion of lithium into the graphite electrode towards the end of the lithiation became more and more hindered. A change in the "curvature" of the lithiation curve towards the end of the lithiation was then seen for the 556th lithiation. Such a change, which became more pronounced for the 621st and 671st lithiation, indicates a transfer from the LiC_{12} phase transition plateau to the LiC_6 one. In addition, the first phase transition plateau during the lithiation seen at 20-35 mAh g^{-1} also gradually "disappeared" upon the cycling. These results are in good agreement with the findings of a previous study.[47] It is reasonable to attribute the observed changes in the electrochemical performance to a gradual capacity loss of the graphite electrode. This could stem from diffusion-controlled trapping of lithium in the graphite electrode even

though SEI formation effects are typically used to explain such a capacity fading of a cell.[5][6][47][115] Diffusion-controlled lithium trapping should be considered for two reasons. First, the lithium counter electrode in the half cell should be able to compensate for the capacity associated with SEI layer formation (and maintenance). Second, an increasing interfacial resistance due to a thicker SEI layer would have affected the shapes of the lithiation and delithiation curves equally, which is not seen in **Figure 4.1**a. On the other hand, the trapping effect could lead to an increasing lithium concentration in the graphite electrode. This would hinder the lithiation process,[33]–[35] and could thus explain the narrower (and disappearing) first phase transition plateau as well as the earlier appearance of the LiC_6 phase transition plateau.

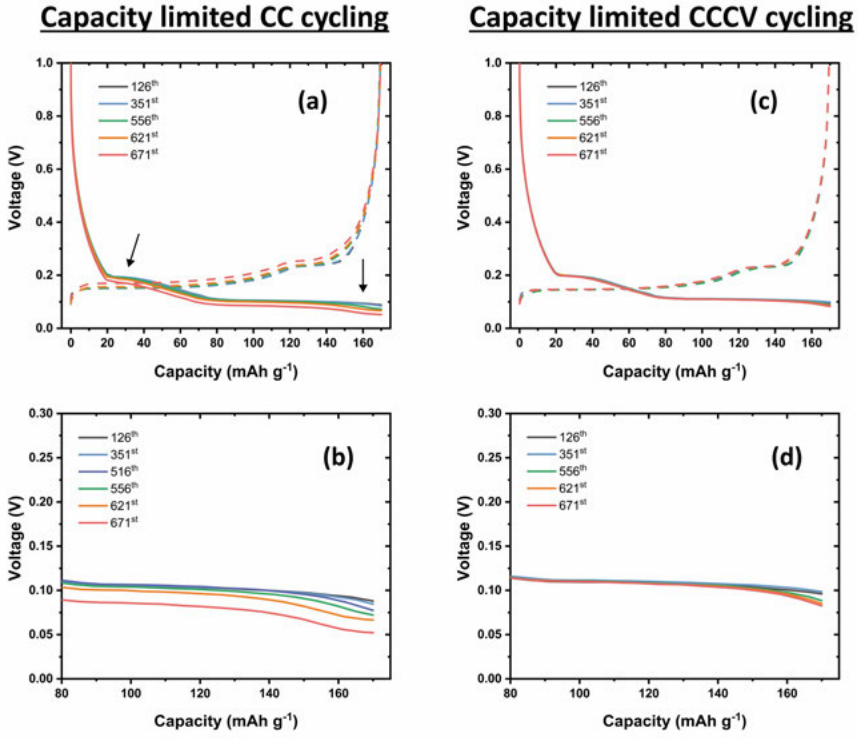

Figure 4.1. CC lithiation and delithiation curves of various cycle numbers for the graphite electrodes in graphite/Li half cells cycled with the capacity-limited (a) CC and (c) CCCV cycling protocols (see the text or **Paper I**). In (a), the arrows point out the major changes in the shapes of the lithiation curves. Magnified views of the lithiation curves towards the lithiation capacity limit are presented in (b) and (d) for the CC and CCCV cycling protocols, respectively. The lithiation curve of the 516th cycle is also included in (b) to better demonstrate the "trend" (see the text). The lithiation capacity limit was 170 mAh g^{-1}, and the current for the CC steps was 35 mA g^{-1}.

The abovementioned curvature changes in the lithiation curves were, however, not seen when a CV delithiation step at 1 V was included on every fifth cycle during the cycling (i.e., when using the CCCV cycling protocol). As can be seen in **Figure 4.1**c and d, the graphite electrode had a much more stable electrochemical performance during the CCCV cycling, although a similar voltage drop towards the end of the lithiation was still seen. Since the only difference between the CC and CCCV cycling protocols was the CV delithiation steps used in the latter, SEI formation and volume expansion effects clearly can not explain the observed performance difference. Instead, a diffusion-controlled lithium trapping effect is the most likely explanation for the gradual performance degradation of the graphite electrodes in the capacity-limited cycling experiments. The improved performance seen with the CCCV cycling protocol can then be attributed to the CV steps decreasing the influence of the trapping effect by increasing the delithiation efficiency.[33]–[35] This will be discussed in more detail in Section 4.1.4.

To further test the lithium trapping hypothesis, the amounts of lithium remaining in the delithiated cycled graphite electrodes were determined by ICP-AES. The results, which are summarized in **Table 4.1**, clearly indicate that a diffusion-controlled lithium trapping effect was present during the capacity-limited cycling of the graphite electrodes, and that the CV steps in the CCCV cycling protocol enabled a certain recovery of the trapped lithium. This is in very good agreement with the electrochemical data and discussion above. As can be seen in **Table 4.2**, up to around 30% of the total accumulated capacity loss could be attributed to the trapped lithium, whereas the remaining 70% should be ascribed to the charge used for the formation and maintenance of the SEI layer during the cycling. While this may explain why SEI formation effects are usually considered to be responsible for the observed capacity losses, the contribution from lithium being trapped in the electrode should clearly not be neglected. More importantly, the trapping effect can directly affect the charge storage capacity of graphite electrodes and potentially cause further issues as described in Section 1.2.2.

Table 4.1. The lithium amounts found in the graphite electrodes before cycling (i.e., in the pristine state) and after 673 and 676 cycles of capacity-limited CC and CCCV cycling, respectively. The corresponding gravimetric capacities of the lithium were calculated according to Faraday's Law (considering $Li^+ + e^- \rightleftharpoons Li$) and based on the graphite mass in the electrodes.

	Graphite mass	Lithium amount	Corresponding capacity
CC (673)	3.72 mg	107.7 µg	111.75 mAh g^{-1}
CCCV (676)	3.75 mg	99.4 µg	102.31 mAh g^{-1}
pristine	-	0.016 µg*	-

*An average value for three pristine electrodes, obtained in a blank measurement.

Table 4.2. The total accumulated capacity losses and the estimated contributions from the trapped lithium and SEI formation/maintenance after 673 and 676 cycles of the capacity-limited CC and CCCV cycling, respectively. The gravimetric capacities are based on the graphite mass presented in Table 4.1. The total (accumulated) capacity loss was calculated as the sum of the differences between the lithiation and delithiation capaci-ties for each cycle.

	Total capacity loss	Trapping capacity loss	SEI capacity loss
CC (673)	365.20 mAh g^{-1}	111.75 mAh g^{-1} (30.6%)	253.45 mAh g^{-1} (69.4%)
CCCV (676)	376.87 mAh g^{-1}	102.31 mAh g^{-1} (27.1%)	274.56 mAh g^{-1} (72.9%)

4.1.2 Lithium trapping and an open-circuit pause

As described in Section 1.2.1, diffusion-controlled lithium trapping can be ascribed to a two-way diffusion phenomenon caused by lithium concentration gradients formed during lithiation and delithiation steps.[33]–[35] In order to reveal the presence of such concentration gradients in the graphite electrode formed during CC lithiation, an EIS experiment was performed during an open-circuit pause after lithiating the electrode to 170 mAh g^{-1}. As can be seen in **Figure 4.2**, the variations in the impedance and open-circuit cell voltage (which could be considered as the open-circuit potential of the graphite electrode) indicate that an equilibration process was taking place during the open-circuit pause. This equilibration process could be attributed to solid-state intra- and inter-particle diffusion of lithium induced by the concentration (or SOC) gradients present within the graphite electrode in multiple directions.[116][117] As can be seen in the photo presented in **Figure 4.3**a, a non-uniform distribution of the reddish color (which represents the LiC_{12} species) further supports the trapping hypothesis regarding inhomogeneous lithiation of the graphite electrode.[43]–[46][118] Such a non-uniform color distribution was, however, not seen when an open-circuit pause of 226 hours was introduced after the lithiation (see **Figure 4.3**b). This indicates that lithium diffused further into the graphite electrode during the open-circuit pause. Such diffusion would also explain the increasing cell voltage with time. Thus, the results presented in **Figure 4.2** and **4.3** clearly demonstrate the presence of lithium concentration gradients (or SOC inhomogeneities) at the end of the lithiation step, which should trigger solid-state lithium diffusion and hence then lead to trapping of lithium in the graphite electrode.

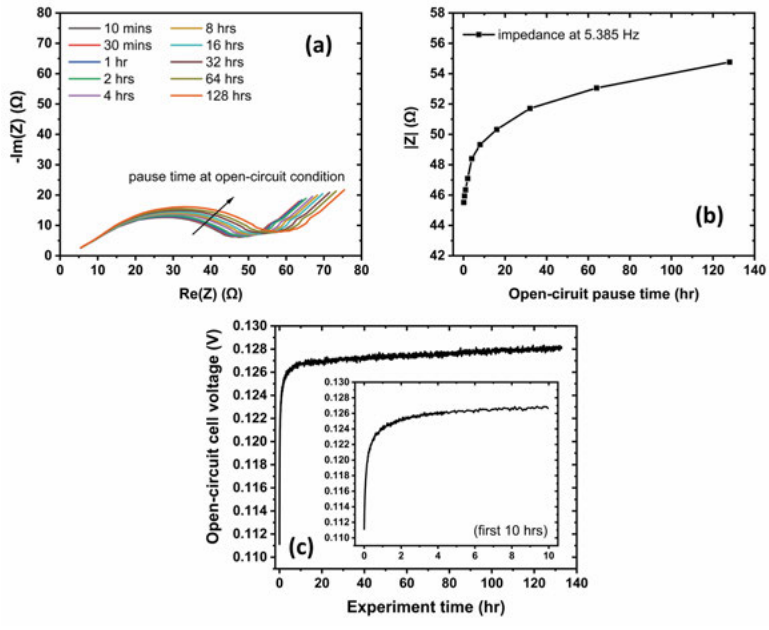

Figure 4.2. Results of the EIS experiment (performed after the graphite electrode underwent CC lithiation to 170 mAh g^{-1}) showing (a) the Nyquist plots obtained after different time during the open-circuit pause, (b) the impedance |Z| at the frequency of 5.385 Hz taken from the data in (a) as a function of the open-circuit pause time, and (c) the open-circuit cell voltage variation during the experiment. In (b), 5.385 Hz was the frequency at which the compressed semicircles in (a) ended. The insert in (c) shows an enlarged view of the data for the first ten hours. Note that the experiment time includes the open-circuit time and the time needed to perform the impedance measurements.

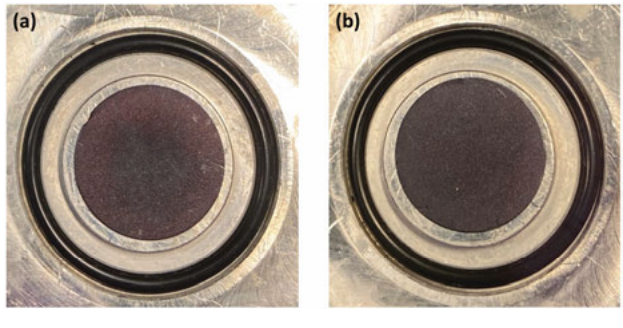

Figure 4.3. Digital photos of the graphite electrodes retrieved from the coin cells disassembled (a) right after CC lithiation to 170 mAh g^{-1} and (b) after an open-circuit pause of 226 hours following the CC lithiation to 170 mAh g^{-1}.

4.1.3 Influence of an open-circuit pause on the subsequent delithiation step

In order to obtain further insights into the diffusion-controlled lithium trapping effect and the concentration gradients, experiments were designed to study the influence of an open-circuit pause on the subsequent delithiation step.

In the open-circuit-pause experiment, an open-circuit pause with an increasing duration of up to 256 hours was introduced between CC lithiation to 170 mAh g^{-1} and CC delithiation to 1 V, and the delithiation capacity obtained after each open-circuit pause was measured (see **Paper I** for more details). As shown in **Figure 4.4**a, the delithiation capacity decreased linearly with the open-circuit pause time raised to the power of 0.7 (i.e., $t^{0.7}$). This indicates that the introduction of an open-circuit pause gave rise to a delithiation capacity loss, and that this loss was associated with, at least, one diffusion-controlled phenomenon. Using a simple diffusion model, the capacity loss that should be seen when an open-circuit pause of 256 hours is applied between the CC lithiation and delithiation can be estimated. This can be done by considering the average capacity loss per cycle seen during the long-term capacity-limited CC cycling and the total time prior to the delithiation step with and without the pause (see **Paper I** for the details). Considering the time scale of this experiment and the calculation results, the extra capacity loss seen in the presence of an open-circuit pause should mainly be caused by the diffusion-controlled lithium trapping effect. Due to the concentration gradients present at the end of the lithiation step, lithium should diffuse further into the electrode during the open-circuit pause. With a longer open-circuit pause, more lithium could thus diffuse too far into the electrode to be extracted within the time domain of the subsequent delithiation step.

As described in Section 3.2.2, the ICI method can be used to track the internal resistance, R, and diffusion resistance coefficient, k, somewhat continuously throughout the whole SOC range.[110]–[112] The former is the total resistance of the cell, while the latter reflects the resistance associated with the (solid-state) lithium diffusion in the cell. With the half cells used in this study, the variations in R and k can be used to study changes occurring within the graphite electrodes (i) during the lithiation and delithiation steps in a cycle, (ii) when modifications being made to the cycling, etc. Thus, insights into the diffusion-controlled trapping phenomenon can be gained.

In the pause-ICI experiment, the derived $R_{delithiation}$ and $k_{delithiation}$ values in the presence and absence of an open-circuit pause of 64 hours between CC lithiation to 170 mAh g^{-1} and delithiation to 1 V were compared. As can be seen in **Figure 4.4**b, $R_{delithiation}$ remained higher during the delithiation when the open-circuit pause was included. This finding, which is in good agreement with the EIS results discussed above, can be ascribed to lithium "redistribution" via diffusion due to the concentration gradients present at the end of the lithiation step. In **Figure 4.4**c, a rapid increase in $k_{delithiation}$ towards the end of

the delithiation step was seen for a standard cycle (i.e., without the open-circuit pause). This indicates that it was difficult to extract the final portion of the inserted lithium due to diffusion hinderance, in good agreement with the diffusion-controlled lithium trapping hypothesis.[33]–[35] The lithium extraction became even more difficult in the presence of the open-circuit pause as the increase in $k_{delithiation}$ towards the end of the delithiation step became much more dramatic. This observed phenomenon is in good agreement with the delithiation capacity losses seen in **Figure 4.4**a.

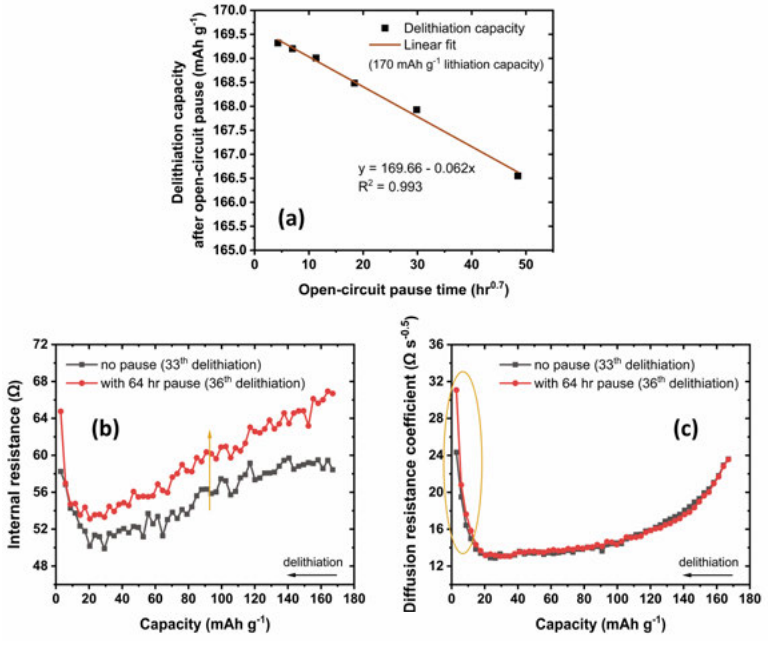

Figure 4.4. (top) Open-circuit-pause experiment results showing (a) the delithiation capacity, obtained in the presence of an open-circuit pause between CC lithiation to 170 mAh g^{-1} and CC delithiation to 1 V, as a function of the pause time raised to the power of 0.7 (i.e., $t^{0.7}$). (bottom) Pause-ICI experiment results showing the derived (b) internal resistance and (c) diffusion resistance coefficient as a function of the SOC during the delithiation step with and without an open-circuit pause of 64 hours between the lithiation to 170 mAh g^{-1} and delithiation to 1 V. The oval in (c) highlights the dramatic increase in the difference between the $k_{delithiation}$ values close to the end of the delithiation.

4.1.4 Effects of constant-voltage delithiation steps on lithium trapping

In the long-term capacity-limited experiments discussed above, it can be seen that the CCCV cycling protocol significantly reduced the electrochemical performance degradation (due to the trapping effect) of the graphite electrodes. In order to study the effects of the CV steps in more detail, a pause-CV step

experiment was designed. In the experiment, an open-circuit pause with an increasing duration was included between CC lithiation to 170 mAh g^{-1} and CC delithiation to 1 V, and the delithiation capacity obtained during an 8-hour long CV step at 1 V, following the CC delithiation, was measured.

As can be seen in **Figure 4.5**a, most of the delithiation capacity extracted during the CV step was obtained within the first 1.5 hours, and the capacity accumulation rate decreased with time. The good fits of the data collected in the first ten minutes to the integrated Cottrell equation indicate that the capacity and current "drawn" during this period of the CV delithiation step was diffusion controlled (see **Figure 4.5**b). This suggests that the delithitation efficiency can be improved by increasing the total duration of the delithiation, e.g., using a CV step, and that the delithiation capacity depends on the rate at which the lithium in the graphite electrode diffuses towards the electrode surface. The findings are in good agreement with the diffusion-controlled lithium trapping hypothesis.[33]–[35] In addition, the lower delithiation capacity obtained during the CV step in the presence of a longer open-circuit pause is also in very good agreement with the experiment results presented in **Figure 4.2** and **4.4**, as more lithium became inaccessible. Furthermore, the smaller constant in the fitting function seen for a longer open-circuit pause implies more hindered lithium diffusion (see **Figure 4.5**b). This is in perfect agreement with the much higher $k_{delithiation}$ values seen at the end of the delithiation, following the 64-hour long open-circuit pause, in **Figure 4.4**c.

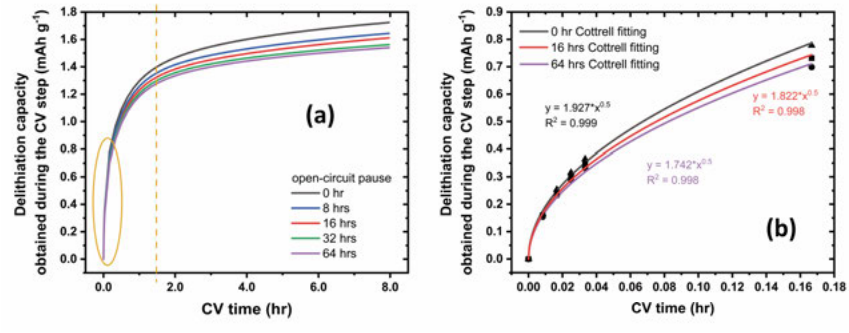

Figure 4.5. Pause-CV step experiment results showing (a) the delithiation capacity obtained during an 8-hour long CV step at 1 V when an open-circuit pause of various durations was applied between CC lithiation to 170 mAh g^{-1} and CC delithiation to 1 V, and (b) the data points collected in the first ten minutes (i.e., from the highlighted region in (a)) for an open-circuit pause of 0, 16 and 64 hours, respectively, together with the fittings of the data to the integrated Cottrell equation. The dash line in (a) marks the CV step time of 1.5 hours.

4.2 Early mitigation of diffusion-controlled lithium trapping for improved high-rate cycling of full cells

In Chapter 4.1, the presence and cause of a diffusion-controlled lithium trapping effect in conventional graphite electrodes have been demonstrated and studied. In this chapter, the results of a series of cycling experiments, designed to study the impact of the trapping effect on the high-rate cycling performances of NMC811/graphite full cells, are presented and discussed. In addition, a key factor for the realization of stable and prolonged cell cycle life under high-rate cycling is proposed and discussed. Details can be found in **Paper II**.

4.2.1 Impact of diffusion-controlled lithium trapping in graphite electrodes on the high-rate cycling performances

Four different cycling protocols were designed to study the impact of diffusion-controlled lithium trapping in graphite electrodes on the cycling performances of NMC811/graphite full cells during 1C cycling. The protocols are summarized in **Table 4.3**. The CC (formation) protocol involved initial CC cycling at C/10 and C/5 followed by cycling at 1C, whereas the CC protocol only involved 1C cycling. In the other two protocols, CC cycling at 1C was adopted together with a CV discharge step at 2.8 V on either every cycle (i.e., CV (1)) or every fifth cycle (i.e., CV (5)).

Table 4.3. The four different cycling protocols.

Protocols	**Cycle #1 and #2**	**Cycle #3 and #4**	**Following cycles**
CC (formation)	CCCV charge: C/10 until 4.2 V 4.2 V until current ≤ C/100 CC discharge: C/10 until 2.8 V	CCCV charge: C/5 until 4.2 V 4.2 V until current ≤ C/50 CC discharge: C/5 until 2.8 V	CC charge and discharge at 1C between 2.8 and 4.2 V
CC	CC charge and discharge at 1C between 2.8 and 4.2 V	CC charge and discharge at 1C between 2.8 and 4.2 V	CC charge and discharge at 1C between 2.8 and 4.2 V
CV (1)	CC charge and discharge at 1C between 2.8 and 4.2 V **with a 1.5-hour long CV discharge step at 2.8 V***	CC charge and discharge at 1C between 2.8 and 4.2 V **with a 1.5-hour long CV discharge step at 2.8 V***	CC charge and discharge at 1C between 2.8 and 4.2 V **with a 1.5-hour long CV discharge step at 2.8 V***
CV (5)	CC charge and discharge at 1C between 2.8 and 4.2 V	CC charge and discharge at 1C between 2.8 and 4.2 V	CC charge and discharge at 1C between 2.8 and 4.2 V **with a 6-hour long CV discharge step at 2.8 V* on every fifth cycle (i.e., 5th, 10th, 15th…)**

*The CV discharge step was applied after the CC discharge to 2.8 V.

The effect of diffusion-controlled lithium trapping in the graphite electrode can be readily seen on the first cycle (see **Figure 4.6**a and b). Despite the fact that a higher charge capacity was obtained for the cells cycled with the CC (formation) protocol due to the adopted formation procedure, the accumulated capacity loss after the first cycle was nearly identical to that seen for the cells cycled with the CV (1) protocol. On the other hand, higher accumulated capacity losses were seen for the cells cycled with the CC and CV (5) protocols. As already explained in Chapter 4.1 and **Paper I**, CV discharge steps can be used to increase the efficiency of discharge (i.e., delithiation of the graphite electrode).[119] Since the only difference between the CV (1) and CC or CV (5) protocols on the first cycle was the CV discharge step, the differences between the accumulated capacity losses seen in **Figure 4.6**b should mainly result from the trapping effect.

Except for the cells cycled with the CV (1) protocol, which will be discussed later in Section 4.2.2, the amounts of trapped lithium escalated in the following cycles of 1C cycling, as is reflected in the rapidly increasing accumulated capacity losses. For the cells cycled with the CC (formation) and CC protocols, the accumulated capacity losses roughly reached their maxima after 5-6 cycles of 1C cycling as the corresponding charge capacities reached their minima (see **Figure 4.6**a and b). The decreases in the accumulated capacity losses afterward indicate that the discharge capacities at these points became larger than the charge capacities. This can be explained by the "saturation" of trapped lithium within the graphite electrodes, which resulted in concentration profiles that facilitated the delithiation of the graphite electrodes due to favored lithium diffusion towards the electrode surface.[35] The results thus indicate that the trapping effect is a general phenomenon regardless of whether a conventional formation procedure is used or not.

In contrast, the 6-hour long CV discharge step at 2.8 V (following the CC discharge) included in the CV (5) protocol on the 5th cycle significantly decreased the accumulated capacity loss and gave rise to considerably "recovered" charge capacity on the next cycle (see **Figure 4.6**a and b). As can be seen in **Figure 4.6**d, the CC charge step on the 6th cycle was notably facilitated by the extraction of trapped lithium during the previous CV step.[119] Nevertheless, as also can be seen in **Figure 4.6**a and b, the accumulated capacity loss on the 6th cycle increased and the charge capacity on the 7th cycle decreased. This effect was caused by the fact that the extensive delithiation of the graphite electrode on the 5th cycle subsequently facilitated deep diffusion of lithium into the electrode and hence lithium trapping.[119] On the following cycles, the increase in the accumulated capacity loss after each CV discharge step, however, became smaller and smaller, and the CV discharge capacities also decreased (see **Figure 4.6**e). This implies that a "steady state" was gradually attained in the cells, which will be discussed further in Section 4.2.2. Similar behaviors were also seen for the cells cycled with the CC (formation) and CC protocols, albeit with much lower charge capacities and much higher

accumulated capacity losses. The results thus clearly indicate that the lithium trapping effect has significant impact on the high-rate cycling performances of the NMC811/graphite cells.

As can been seen in **Figure 4.6**c, the cells cycled with the CV (5) protocol outperformed those cycled with the CC (formation) protocol during long-term cycling, yielding a 43% higher discharge capacity on the 299th cycle. This indicates that the conventional low-rate formation cycling is less effective in preparing cells for high-rate cycling. Development of formation procedures for high-rate cycling should instead consider the adoption of sufficiently long (see **Figure 4.6**e) CV discharge steps with a suitable repetition frequency.

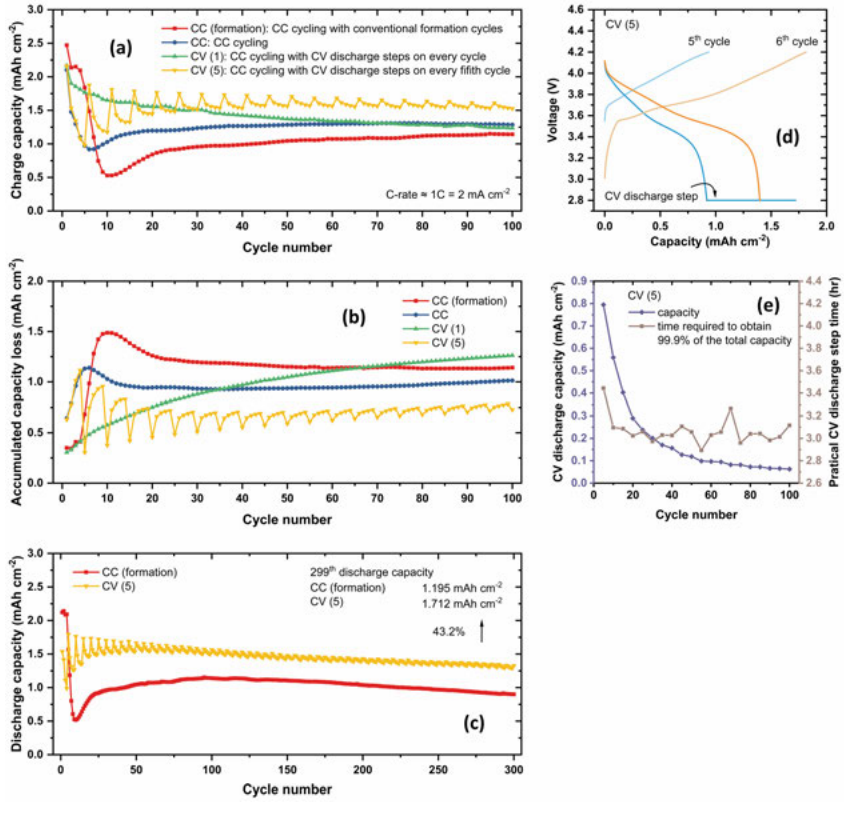

Figure 4.6. Performances of NMC811/graphite cells cycled with the four different protocols summarized in **Table 4.3**. (a) and (b) The charge capacities and the accumulated capacity losses as a function of the cycle number, respectively. The accumulated capacity loss was calculated as the sum of the differences between the charge and discharge capacities for each cycle. (c) The discharge capacities as a function of the cycle number during long-term cycling with the CC (formation) and CV (5) protocols. Note that the CC (formation) protocol included initial formation cycles at C/10 and C/5. (d) Charge and discharge curves for the 5th and 6th cycles of a cell cycled with the CV (5) protocol. (e) The capacity obtained during the CV discharge step and the "practical" duration of the step as a function of the cycle number for the cells cycled with the CV (5) protocol.

4.2.2 Establishing a proper lithium concentration profile in the graphite electrode

In order to further explain the experiment results, the lithium concentration profiles in the graphite electrodes should be considered. Since graphite electrodes contain no lithium in their pristine state, it is reasonable to assume that a proper steady-state concentration profile needs to be established in the electrode in order to obtain long-term cycling stability of the battery cell. Such a steady-state concentration profile should depend on the cycling rate, as the latter will affect the concentration gradients formed in the electrode.

For the cells cycled with the CC (formation) and CC protocols, diffusion-controlled trapping of lithium during the initial cycles gradually built up lithium concentration profiles in the graphite electrodes. As mentioned in the previous section, at some point, the concentration profiles resulted in favored diffusion of lithium within the graphite electrodes to the electrode surface and then subsequently enabled steady-state behaviors to be gradually reached (see **Figure 4.6**a and b). The results for the CC (formation) cycling show that this type of cycling resulted in a higher accumulated capacity loss during 1C cycling compared to the CC and also CV (5) protocols. This is most likely due to the thicker lithium diffusion layers generated during the initial formation cycling at C/10 and C/5 that "activated" a larger portion of the electrode.

As shown in **Figure 4.6**a and b, significantly different behaviors were seen with the CV (5) and CV (1) protocols. As explained in the previous section, the CV discharge step was used on every cycle in the CV (1) case, rather than on every fifth cycle as in the CV (5) case. The continuously decreasing charge capacity and continuously increasing accumulated capacity loss seen in the CV (1) case indicate that the CCCV discharge steps then were "too efficient". This made it difficult to generate lithium concentration gradients in the graphite electrode, analogous to those formed during the first five to ten cycles in all the other cases, which most likely hindered the establishment of a steady state. The fact that the highest charge capacity and lowest accumulated capacity loss were seen for the CV (5) protocol indicates that, with the suitable application of the CV discharge steps, a proper steady-state lithium concentration profile could be obtained faster than with all the other protocols. Overall, the experiment results presented in **Figure 4.6** thus indicate that the best long-term performances were obtained when a proper lithium concentration profile was formed in the graphite electrode during the initial part of the cycling, and that this was difficult to attain when a CV delithiation step was used on every cycle.

4.3 Influence of the particle size on diffusion-controlled lithium trapping in silicon nanoparticle based electrodes

In this chapter, the results of a series of electrochemical half-cell experiments using three different silicon nanoparticle based electrodes (i.e., the SiNP100, SiNP50-80 and SiNP≤50 electrodes, see Section 3.1) are presented and discussed, in an attempt to identify and specify the influence of the particle size on the diffusion-controlled trapping effect. In addition, the importance of carefully designing different cycling protocols is also briefly discussed. Details can be found in **Paper III**.

4.3.1 Diffusion-controlled lithium trapping in the three different silicon electrodes

Long-term capacity-limited CC cycling experiments were first conducted to compare the cycling performances of the three different silicon electrodes. In these experiments, the cells were cycled between 0.01 and 1 V with a lithiation capacity limit of 1200 mAh g^{-1} (i.e., the lithiation step was terminated when either the capacity limit was reached or the cell voltage dropped to the cut-off voltage of 0.01 V).

As can be seen in **Figure 4.7**a, the SiNP50-80 electrode had the longest cycling lifetime, in terms of sustaining the 1200 mAh g^{-1} lithiation capacity, followed by the SiNP≤50 and then SiNP100 electrodes. Considering the significantly high accumulated capacity losses seen for all the three electrodes, it is reasonable to assume that their cycling performances were influenced by diffusion-controlled lithium trapping,[33]–[35] although, most likely, to different degrees.

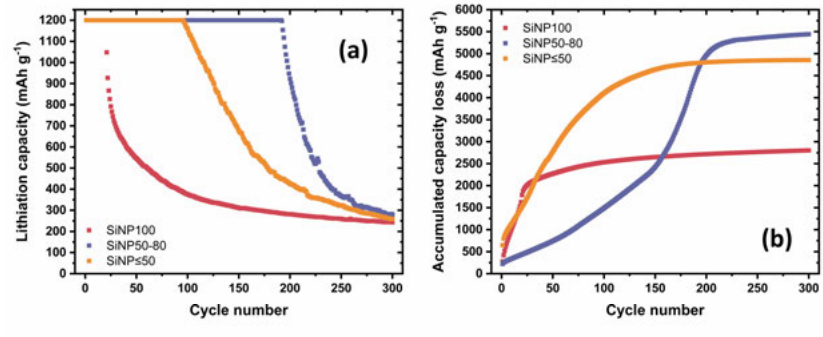

Figure 4.7. Capacity-limited CC cycling performances of the three different silicon electrodes in Si/Li half cells, showing (a) the lithiation capacities and (b) the accumulated capacity losses as a function of the cycle number. The accumulated capacity loss was calculated as the sum of the differences between the lithiation and delithation capacities for each cycle. The lithiation capacity limit was 1200 mAh g^{-1}, and the currents were 178.95 and 357.9 mA g^{-1} for the first and following cycles, respectively.

The lithium trapping hypothesis is supported by the observed CC lithiation curves in the cycling experiments. As can be seen in **Figure 4.8**, when comparing the shapes of the lithiation curves of an early cycle (e.g., the 11th cycle) with those of a few later cycles, it is clear that all the three different silicon electrodes experienced increasing lithiation hindrance (see Section 4.1.1). This can be attributed to the electrodes being gradually filled up with trapped lithium during the cycling.[34] As a result, at some point, the electrodes could no longer be lithiated to 1200 mAh g^{-1} and the lithiation capacities were then instead determined by how soon the cells reached the cut-off voltage of 0.01 V (see **Figure 4.7**a). This is further supported by the ICP-AES measurements which show that there were significant amounts of lithium in the delithiated cycled electrodes (see **Table 4.4**). Such amounts of lithium can clearly be explained only by the lithium trapping effect. Here, it is also worth pointing out that the lithiation capacities of the three different electrodes all dropped to around 250 mAh g^{-1} after 300 cycles (see **Figure 4.7**a). This may indicate that they all reached a certain "equilibrium" as discussed in Section 4.2.

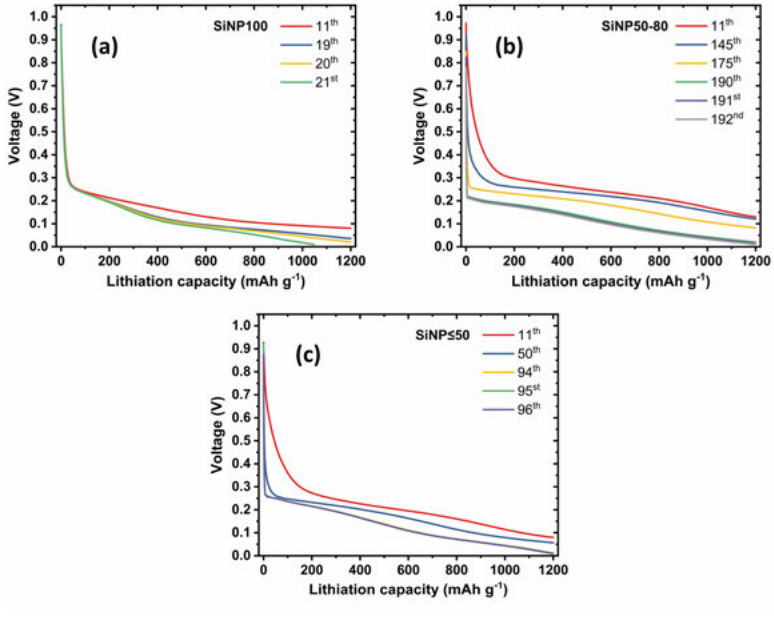

Figure 4.8. CC lithiation curves of various cycle numbers seen for the (a) SiNP100, (b) SiNP50-80, and (c) SiNP≤50 electrodes in Si/Li half cells during capacity-limited CC cycling experiments (see the text and also **Figure 4.7**). Note that the SiNP100, SiNP50-80 and SiNP≤50 electrodes started to fail to reach the lithiation capacity limit of 1200 mAh g^{-1} since the 21st, 192nd and 96th cycles, respectively. Note also that the last three curves in (b) and (c) almost overlap with each other.

Table 4.4. The capacities corresponding to the amounts of lithium found in the three different silicon electrodes after the long-term capacity-limited CC cycling as well as the total accumulated capacity losses (see **Figure 4.7**). The corresponding capacities were calculated according to Faraday's Law (considering $Li^+ + e^- \rightleftharpoons Li$) and based on the silicon mass in the electrodes.

	Corresponding capacity	Total accumulated capacity loss
SiNP100	2799.6 ± 108.7 mAh g^{-1}	2800.8 mAh g^{-1}
SiNP50-80	4686.5 ± 93.5 mAh g^{-1}	5442.5 mAh g^{-1}
SiNP≤50	4803.7 ± 96.0 mAh g^{-1}	4855.9 mAh g^{-1}

ICI experiments were also conducted to gain more insights. In analogy with the graphite electrode case discussed in Section 4.1.3, the ICI method (see Section 3.2.2) was used to derive the diffusion resistance coefficients, k, to study the diffusion of lithium in the three different electrodes. As can be seen in **Figure 4.9**, for all the three electrodes, $k_{delithiation}$ increased markedly during the delithiation, especially towards the end of it. This indicates that extracting the inserted lithium, especially the final portion, was difficult, most likely as a fraction of the inserted lithium could diffuse further into the electrode due to the presence of concentration gradients.[33]–[35] The latter relocation of lithium resulted in a small portion of the inserted lithium that diffused too deep into the electrode being trapped in the electrode (on every cycle). As the lithium concentration in the electrode gradually increased during the cycling, the charge storage capacity of the electrode consequently decreased.

Based on the experiment results discussed above, it can be concluded that the observed differences in the cycle life performances of the SiNP100, SiNP50-80 and SiNP≤50 electrodes should result from the differing influence of diffusion-controlled lithium trapping. The latter is very likely related to the different sizes of the silicon nanoparticles used in the electrodes.

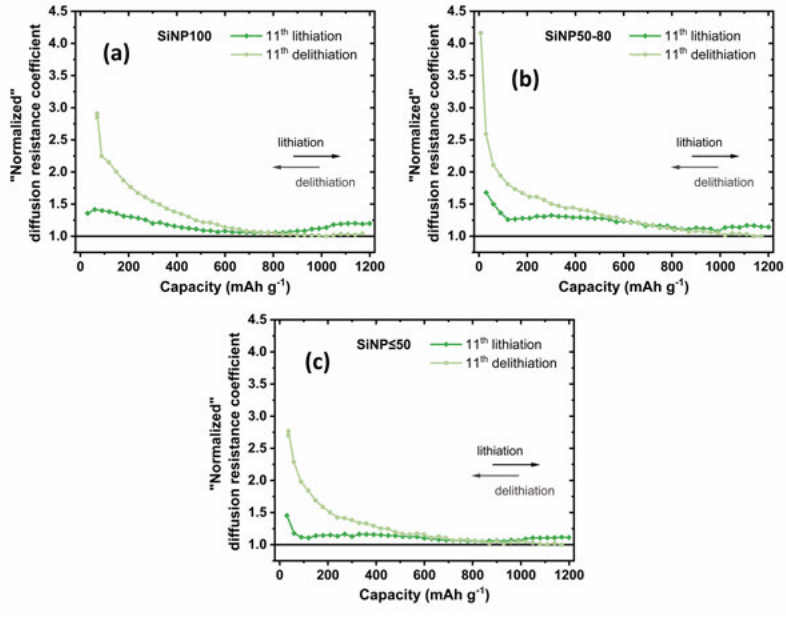

Figure 4.9. ICI experiment results showing the "normalized" diffusion resistance coefficients, k, for the (a) SiNP100, (b) SiNP50-80, and (c) SiNP≤50 electrodes, respectively. The "normalized" k values were calculated by dividing the experimentally derived k values by the smallest value seen for each electrode to better demonstrate the variations of k. The lithiation capacity was limited to 1200 mAh g^{-1}.

4.3.2 Influence of the silicon nanoparticle size

As briefly explained in Section 1.2.3, diffusion-controlled lithium trapping should be considered at the electrode level. This should naturally include the liquid phase (i.e., the electrolyte (in the pores of the electrode)) and the solid phase (i.e., the composite matrix of the electrode coating itself). Details concerning the following discussion can be found in **Paper III**.

By calculation, it can be shown that the lithiation of the silicon nanoparticle based electrodes relies heavily on the Li^+ flux from the lithium-metal counter electrodes in the half cells. The potential issue with the Li^+ flux can be expected to be inhomogeneous lithiation with silicon located closer to the electrode-separator interface being lithiated first.[120][121] This and the fact that most likely not all the silicon nanoparticles had direct contact with the electrolyte clearly suggest that the electrode microstructure (i.e., how the nanoparticles are distributed, connected and packed in the composite matrix of the electrode) should greatly affect the (de)lithiation behaviors of the electrodes. As a combined result of the inhomogeneous lithiation and slow (inter-particle) solid-state lithium diffusion, lithium concentration gradients should be generated in the electrodes, involving long diffusion paths. This should serve as the basis for the diffusion-controlled lithium trapping effect seen for the silicon

nanoparticle based electrodes. It can therefore be expected that the influence of the trapping effect should depend on the electrode microstructure. This may explain the different CC cycling performances seen for the three electrodes (see **Figure 4.7**). As can be seen in **Figure 4.10**, the SiNP100, SiNP50-80 and SiNP≤50 electrodes indeed had different microstructures. This is actually not surprising, since it is well-known that silicon particles of different sizes have different tap densities.[26][122][123] It is thus concluded that the influence of the trapping effect should be affected by the silicon nanoparticle size, most likely, via its influence on the electrode microstructure.

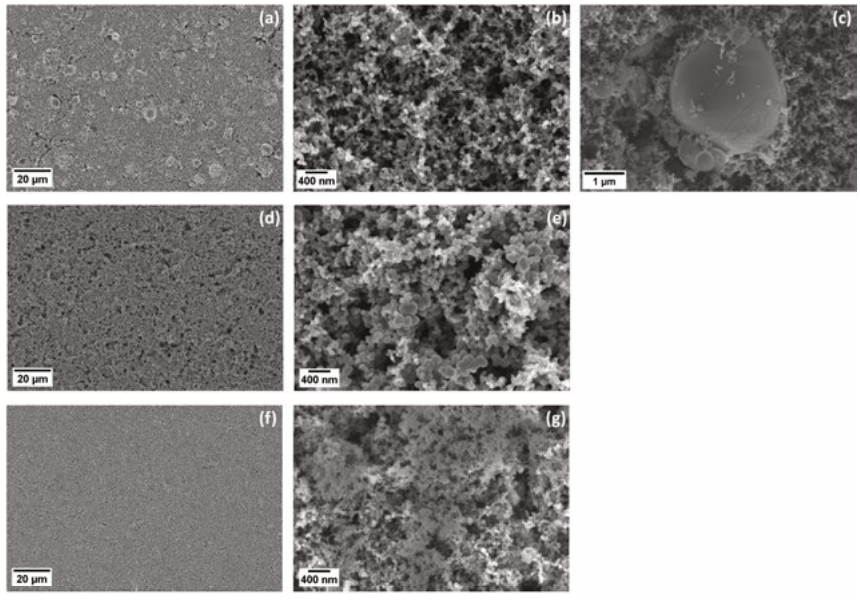

Figure 4.10. SEM images depicting the surface morphologies of the as-fabricated (a-c) SiNP100, (d) and (e) SiNP50-80, and (f) and (g) SiNP≤50 electrodes at different magnifications. Note the inhomogeneous distribution and agglomeration of material particles in the SiNP100 electrode.

4.3.3 Cycling protocols, diffusion-controlled lithium trapping and electrode performances

As described in Section 1.2.1, diffusion-controlled lithium trapping stems from incomplete delithiation of the electrode. To decrease the influence of the trapping effect and thus improve the electrode performances, cycling protocols that can enable higher delithiation efficiencies should hence be used. This can be done by, e.g., including CV delithiation steps (as already shown for graphite electrodes in Section 4.1 and 4.2) or adopting "asymmetric" cycling (i.e., fast lithiation in combination with slow delithiation). The former approach aims at extracting trapped lithium regularly during the cycling, while the latter aims at directly decreasing the amount of trapped lithium on each

cycle by limiting the lithium diffusion "depth" during the lithiation and providing more time for lithium to diffuse out during the delithiation.

As can be seen in **Figure 4.11**, the choice of cycling protocol had pronounced impacts on the electrode performances. However, it is immediately evident that none of the protocols can be considered optimal for all the three different silicon nanoparticle based electrodes. For example, although using the asymmetric CC cycling protocol greatly decreased the accumulated capacity loss seen for the SiNP100 electrode, its cycle lifetime (in terms of sustaining the 1200 mAh g^{-1} lithiation capacity) was actually shortened. Moreover, although the SiNP≤50 electrode cycle lifetime was extended when using the CCCV (every third cycle) cycling protocol, the lithiation capacity retention thereafter was worsened. This indicates that it is crucial to individually customize the cycling protocols for different electrodes.

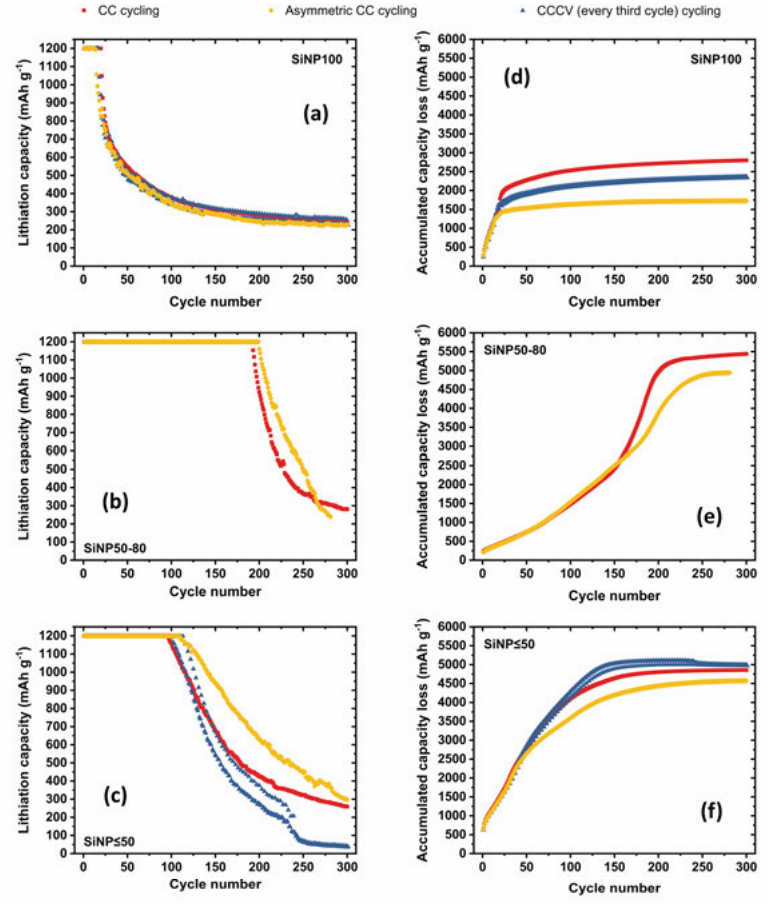

Figure 4.11. Capacity-limited cycling performances of the (a) and (d) SiNP100, (b) and (e) SiNP50-80, and (c) and (f) SiNP≤50 electrodes in Si/Li half cells cycled with different protocols (see **Paper V** for the details). Note that the CC cycling data is taken directly from **Figure 4.7**.

4.4 Stabilizing the cycling of lithium-metal electrodes via the application of a potentiostatic stripping pulse

It is well-known that lithium deposition is affected by the preceding lithium stripping, especially if one starts the cycling with the latter.[67]–[69][124] The idea here is that if more homogeneous lithium stripping can be achieved, it may lead to more homogeneous lithium deposition by improving the homogeneity of the nucleation. As mentioned in the Introduction, a fundamental problem with inhomogeneous lithium stripping is that it takes place predominantly at the most electrochemically active sites on the lithium electrode surface during a CC stripping step.[66]–[69] To circumvent this problem, a potentiostatic stripping pulse could be included before the conventional CC stripping step to first "activate" the entire electrode surface so that the stripping process can take place more homogeneously on the surface.

In this chapter, the effects of the application of potentiostatic stripping pulses on electrochemical lithium stripping and subsequent deposition in conventional 1.0 M $LiPF_6$ electrolytes are demonstrated and discussed. Details can be found in **Paper IV**.

4.4.1 Influence of the potentiostatic stripping pulse height on the subsequent lithium stripping

In order to find a suitable pulse height for the potentiostatic stripping pulse, a series of experiments were conducted to compare the obtained LME surface morphologies after the first CC stripping step, in the presence of a preceding one-second long potentiostatic stripping pulse with various pulse heights. Note that in every experiment there was an open-circuit pause of 100 ms between the stripping pulse and the CC stripping step to allow the generated Li^+ concentration profile at the electrode surface to relax.[67][125]

The electrochemical data and the corresponding SEM images with the analyses of pit size distributions and pit areal densities can be seen in **Figure 4.12**. The SEM images shown in **Figure 4.12**a, k and l illustrate the typical inhomogeneous stripping of LMEs with the formation of randomly distributed pits and surface regions that remain almost intact. Interestingly, even more inhomogeneous surface morphologies were obtained when the applied preceding pulse had a low pulse height (i.e., 0.05 or 0.1 V) (See **Figure 4.12**b and c). This indicates that the 0.05 and 0.1 V pulses in fact caused the lithium stripping to become more confined to a few sites on the electrode surface. However, when the pulse height was further increased from 0.2 to 2 V, smaller average pit sizes with higher pit areal densities and more homogeneous pit distributions were obtained (see **Figure 4.12**d-j). A strikingly different surface morphology was observed when a potentiostatic stripping pulse with a pulse height of 4 V was applied (compare **Figure 4.12**m and n to k and l). The pulse

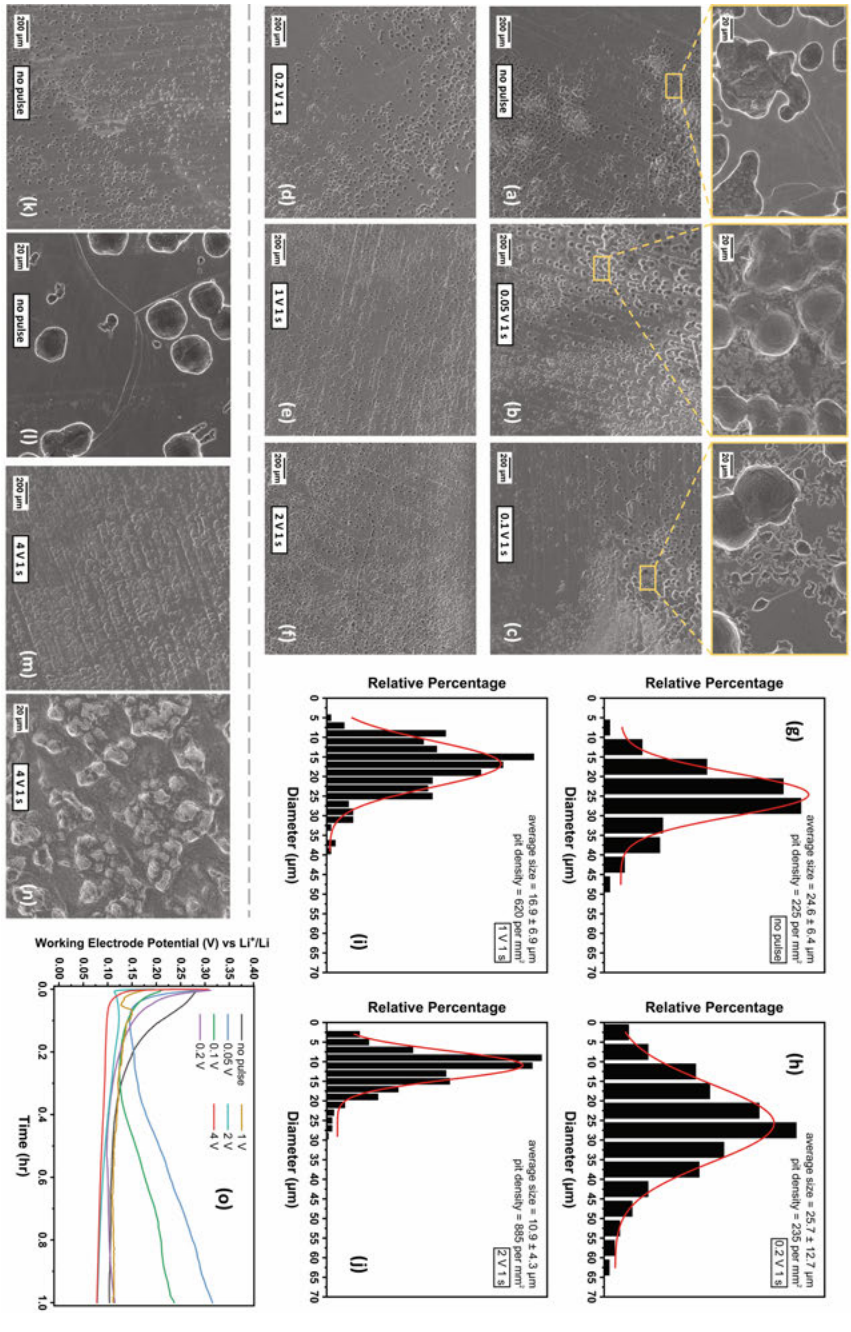

Figure 4.12. SEM images depicting the LME surfaces after the first CC stripping step (a), (k) and (l) in the absence, and presence of a preceding one-second long potentiostatic stripping pulse with a pulse height of (b) 0.05 V, (c) 0.1 V, (d) 0.2, (e) 1 V, (f) 2 V, and (m) and (n) 4 V, respectively. The corresponding analyses of pit size distributions and pit areal densities are summarized in (g-j). Chronopotentiograms seen for the first CC stripping step (i.e., 1.0 mAh cm^{-2} at 1.0 mA cm^{-2}) are presented in (o).

clearly triggered a more homogeneous and more two-dimensional stripping behavior during the subsequent CC stripping step as shallower and interconnected "depressions" were formed, instead of well-defined pits that were larger, deeper, and randomly distributed.

The pulse height of the potentiostatic stripping pulse also influenced the shape of the chronopotentiogram seen for the subsequent CC stripping step (see **Figure 4.12**o). For a sufficiently low pulse height (i.e., 0.05 or 0.1 V), the increase in the potential (i.e., increasing overpotential for electrochemical stripping of lithium) implies that additional pit formation had to take place to support the applied current. This may explain the special surface morphology features seen in **Figure 4.12**b and c. On the other hand, the application of the 4 V stripping pulse resulted in a chronopotentiogram featuring a significant potential drop in the beginning of the CC stripping step followed by a rather steady stripping potential during the rest of the step (see the red curve in **Figure 4.12**o). In contrast, without the stripping pulse, the potential decreased slowly with time (see the black curve in **Figure 4.12**o), indicating an increasing electroactive surface area due to the growth of the relatively large pits.

The findings discussed above thus indicate that the LME surface could be considered as a surface possessing a range of sites with different electrochemical activities (or potentials) toward stripping, in analogy with the model used in the context of electrodeposition of metals.[59][60] Under normal CC conditions, lithium stripping only takes place at the most electrochemically active sites on the lithium electrode surface, yielding only a few but large pits.[69] The application of a potentiostatic stripping pulse with a sufficiently high pulse height can make more sites more electrochemically active. As a result, during the subsequent CC stripping step, more sites are involved in the stripping process, which leads to the formation of smaller and more homogeneously distributed pits or even the depressions seen for the 4 V stripping pulse.

4.4.2 Effects of the potentiostatic stripping pulse

In order to gain more insights into the effects of the potentiostatic stripping pulse, the surface morphologies of the LMEs subjected to different stripping pulses only were studied. As can be seen in **Figure 4.13**a and b, a large number of homogeneously distributed long and tiny pits were obtained after the application of the 4 V stripping pulse, while no obvious feature could be observed on the surface of the LME subjected to the 0.05 V pulse. In addition, the SEM images shown in **Figure 4.13**c and d indicate that the long and tiny pits seen in **Figure 4.13**b were gradually formed during the one-second long stripping pulse (i.e., the pit formation was a progressive rather than instantaneous process). This may be because the actual overpotential imposed by the 4 V stripping pulse was still not high enough to activate the entire electrode surface instantaneously. Here it should be recalled that it should be rather difficult to polarize a LME immersed in an electrolyte containing 1.0 M Li^+, and that the

presence of a large iR drop would decrease the potential actually reached at the lithium working electrode. Experimentally, it was difficult to apply a pulse with a pulse height higher than 4 V due to the large current already produced by the latter. Nevertheless, the results presented in **Figure 4.12** clearly show that a potentiostatic stripping pulse of 4 V for 1 s was able to mitigate the active sites problem to some extent.

As can be seen in **Figure 4.13**c, the LME surface after the first CC stripping step with a preceding stripping pulse of 4 V for 10 ms had a less homogeneous distribution of pits/depressions than that seen in **Figure 4.12**m when a pulse of 4 V for 1 s was used. Based on the results presented in **Figure 4.12** and **4.13**a-d, the effects of a potentiostatic stripping pulse with a pulse height of 4 V and a duration of 1 s can be concluded as follows. The stripping pulse resulted in the formation of a great number of homogeneously distributed and well-developed tiny pits. This allowed the following CC stripping to be better controlled and take place more homogeneously on the surface.

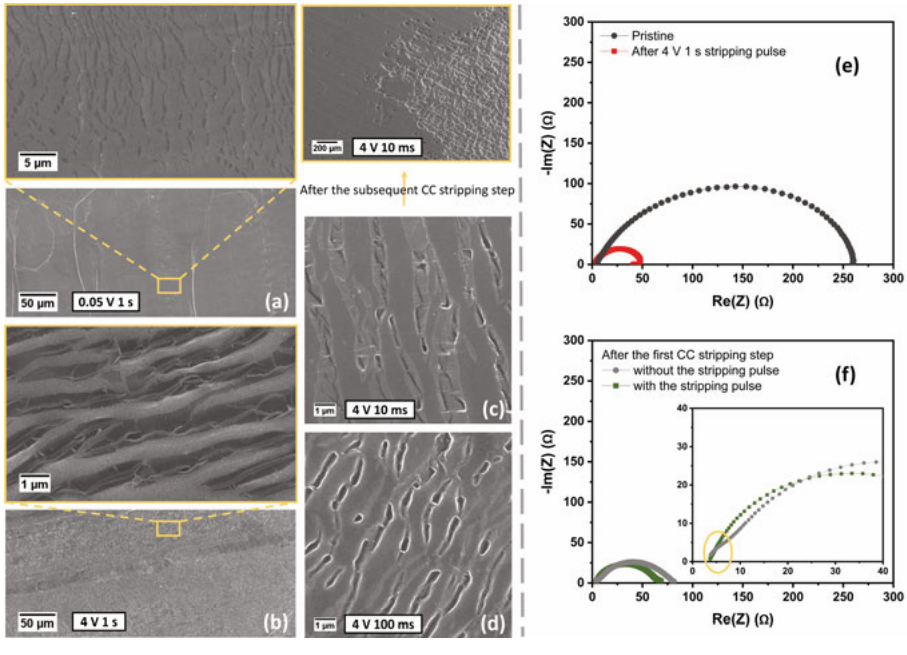

Figure 4.13. (left) SEM images depicting the LME surfaces obtained after applying only a potentiostatic stripping pulse with a pulse height and duration of (a) 0.05 V for 1 s, (b) 4 V for 1 s, (c) 4 V for 10 ms, and (d) 4 V for 100 ms, respectively. The electrode surface seen after the subsequent CC stripping step (i.e., 1.0 mAh cm^{-2} at 1.0 mA cm^{-2}) with the pulse of 4 V for 10 ms is also included in (c). (right) The EIS spectra of the lithium working electrodes obtained (e) before and after the use of a one-second long potentiostatic stripping pulse of 4 V, and (f) after the first CC stripping step with and without the preceding stripping pulse of 4 V for 1 s. The insert in (f) shows a magnified view of the Nyquist plots in which a "shoulder" seen for the LME in the absence of the stripping pulse is highlighted.

The effects of the stripping pulse of 4 V for 1 s are also reflected in the obtained Nyquist plots in EIS experiments. The pristine LME featured a high charge transfer resistance, which could be attributed to the electrochemical reactions (i.e., lithium stripping and deposition) only involving a few sites that were electrochemically more active on the surface (see **Figure 4.13**e). As a result, preferential growth of active pits occurred during the CC stripping step, giving rise to the gradually decreasing potential seen in the chronopotentiogram as well as the obtained surface morphologies (see **Figure 4.12**a, k, l and o). On the other hand, the application of the stripping pulse electrochemically activated the LME surface via the generation of tiny pits, which greatly decreased the charge transfer resistance by diminishing the practical current density. Lithium stripping was then able to take place more homogeneously across the surface, and the potential reached a relatively constant value within a short time (see **Figure 4.12**o). In addition, a "shoulder" was observed in the high frequency range in the Nyquist plot obtained after the first CC stripping step in the absence of the stripping pulse. This implies a less homogeneous surface as well as a less well-defined stripping process,[126] which is in good agreement with the surface morphologies seen in the SEM images.

4.4.3 Improved lithium deposition and cycling performance of the lithium-metal electrode with the stripping pulse

As mentioned above, the lithium deposition behavior is known to be affected by the preceding lithium stripping step.[67][124] The surface morphologies obtained after the subsequent CC deposition step were therefore studied and the results are presented in **Figure 4.14**. It can be clearly seen that a better-controlled lithium stripping process, enabled by the application of the potentiostatic stripping pulse (i.e., 4 V for 1 s), can give rise to homogeneously distributed lithium deposits, whereas lithium was only (apparently) randomly deposited at some regions on the surface in the absence of such a pulse. After comparing the deposition result and the surface morphology obtained after the first CC stripping step shown in **Figure 4.14**c and **Figure 4.12**m, respectively, the mechanism behind the improved deposition could be disclosed. It can be concluded that the densely and homogeneously distributed depressions oxidatively generated during the first CC stripping step in the presence of the potentiostatic stripping pulse of 4 V for 1 s served as preferential nucleation sites which "guided" the deposition of lithium to take place more homogeneously on the surface. On the other hand, without the stripping pulse, the randomly distributed pits obtained after the first CC stripping step confined the subsequent lithium deposition to those pits whereas the other regions remained almost pristine. This resulted in the great inhomogeneity seen in **Figure 4.14**a and b. Even better lithium deposition was enabled by including an additional potentiostatic nucleation/deposition pulse of -1 V for 10 ms prior to the CC

deposition step (see **Figure 4.14**d). Such a nucleation/deposition pulse should increase the lithium nucleation density and hence facilitate the attainment of a more homogeneous deposition result.[67] However, it should be noted that true two-dimensional lithium deposition was still not achieved.

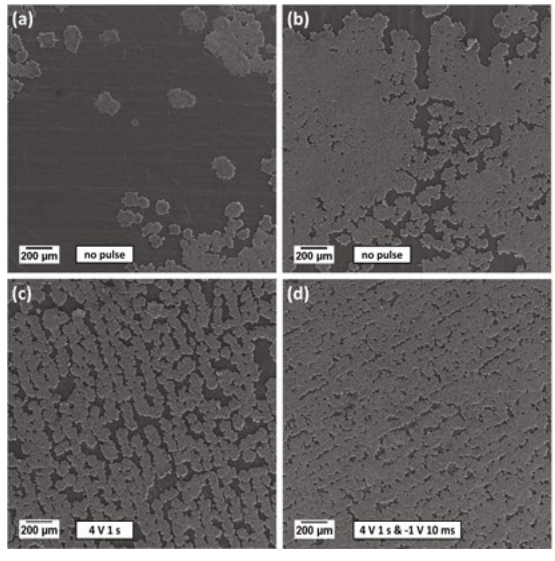

Figure 4.14. SEM images depicting the LME surfaces after the first CC lithium deposition step (i.e., 1.0 mAh cm^{-2} at 1.0 mA cm^{-2}) preceded by the first CC stripping step in the (a) and (b) absence, and (c) presence of the potentiostatic stripping pulse (i.e., 4 V for 1 s) prior to the CC stripping step. (d) The deposition result obtained on the basis of (c) but with an additional potentiostatic nucleation/deposition pulse of -1 V for 10 ms included prior to the CC deposition step.

As can be seen in the chronopotentiograms presented in **Figure 4.15**a, the main difference between the electrochemical performances seen for the LMEs with and without the stripping and nucleation/deposition pulses concerned the first CC stripping step. This clearly indicates that the key to the improved lithium deposition result seen in **Figure 4.14**d was the potentiostatic stripping pulse. With the better-controlled lithium stripping and hence deposition behaviors on the first cycle, the cycling lifetime of the corresponding three-electrode lithium symmetric cell was greatly increased, and the overpotentials, especially during the CC stripping steps, remained relatively low and stable for many cycles (see **Figure 4.15**b and c). The more well-defined oxidation of the lithium deposits was most likely caused by the lithium being more homogeneously deposited on the electrode surface in the first place. This should also have led to less formation of dead lithium. On the other hand, without the pulses, the performance of the LME degraded faster during the cycling with rapidly increasing overpotentials during the CC stripping steps. This resulted in the electrode being converted quicker into a more and more porous structure

with serious dead lithium accumulation, rapidly increasing cell impedances and eventually faster cell failure[69][70][127] (see **Figure 4.15**b and c). However, it should be pointed out that an increase in the overpotential was seen toward the end of every CC stripping step whether or not the pulses were applied, and that both the stripping and deposition overpotentials still increased after certain cycles (see **Figure 4.15**a and b). This indicates that, although the cell cycled with the inclusion of the pulses showed longer cycling lifetime, the LME still gradually became more and more porous due to the formation of new pits and thus some dead lithium at the end of each CC stripping step.[63]

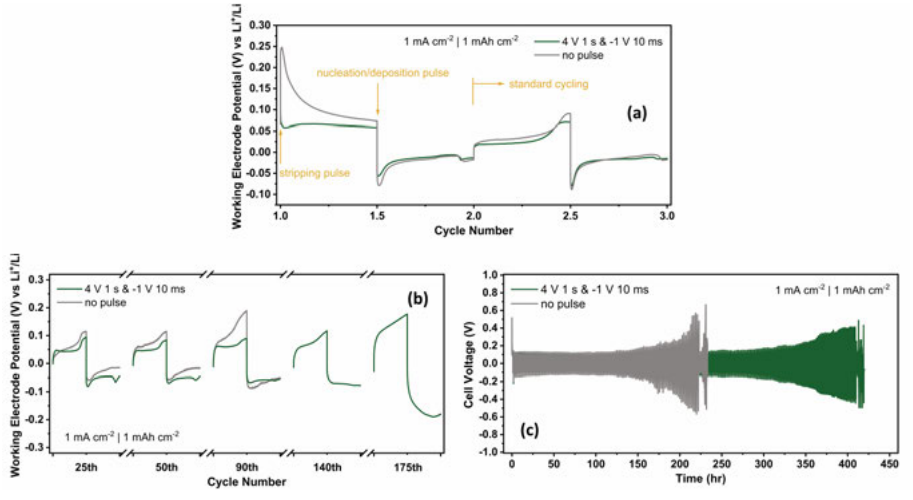

Figure 4.15. Chronopotentiograms showing (a) and (b) the electrochemical performances of the lithium working electrodes seen during the indicated cycles with and without the inclusion of the potentiostatic stripping (i.e., 4 V for 1 s) and nucleation/deposition (i.e., -1 V for 10 ms) pulses, and (c) the long-term cycling performances of the corresponding three-electrode lithium symmetric cells.

4.5 Influence of lithium diffusion into copper current collectors on lithium nucleation/deposition

As mentioned and discussed in Section 1.3.3, Lv et al. proposed that the lithium uptake in copper was most likely due to lithium diffusing into the copper via the grain boundaries.[103] This can potentially have a huge impact on the lithium nucleation when depositing lithium on battery-grade copper foils since such foils are prepared by electrodeposition methods and typically have small grain sizes (down to 0.1 μm or even smaller, see **Figure 4.16**) with a lot of grain boundaries.

In this chapter, the influence of lithium diffusion into copper substrates (i.e., disks punched out from the battery-grade copper foil) on lithium nucleation/deposition on the substrates is demonstrated in a series of lithium deposition experiments performed in conventional EC-based electrolytes. The possibility of using a potentiostatic nucleation pulse to improve the nucleation of lithium and hence attain homogeneous deposition is explored at the same time. Furthermore, a strategy is proposed to decrease the influence of the lithium diffusion, and its effects are discussed. Details can be found in **Paper V**.

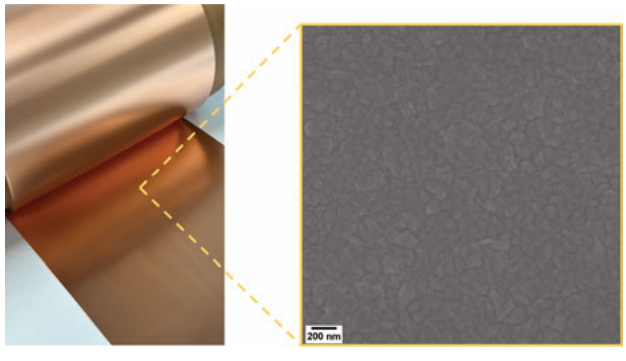

Figure 4.16. A digital photo of the battery-graded copper foil used in **Paper V** with a SEM image depicting the surface morphology of the "matte side".

4.5.1 Lithium deposition on copper current collectors

The morphologies of the deposited lithium obtained on the "pure" copper substrates using the different deposition protocols and electrolytes are shown in **Figure 4.17**. As can be seen in **Figure 4.17**a and b, inhomogeneous deposits were obtained after conventional CC deposition in LP40 electrolyte with the formation of randomly distributed lithium "islands" of different sizes and "networks" of undesirable lithium "threads" on the surface.[100][101] This may stem from the fact that the lithium nuclei were preferentially formed at the most electrochemically favorable sites on the copper surface, in analogy with previous findings for lithium deposition (and stripping) on LMEs.[67][128]

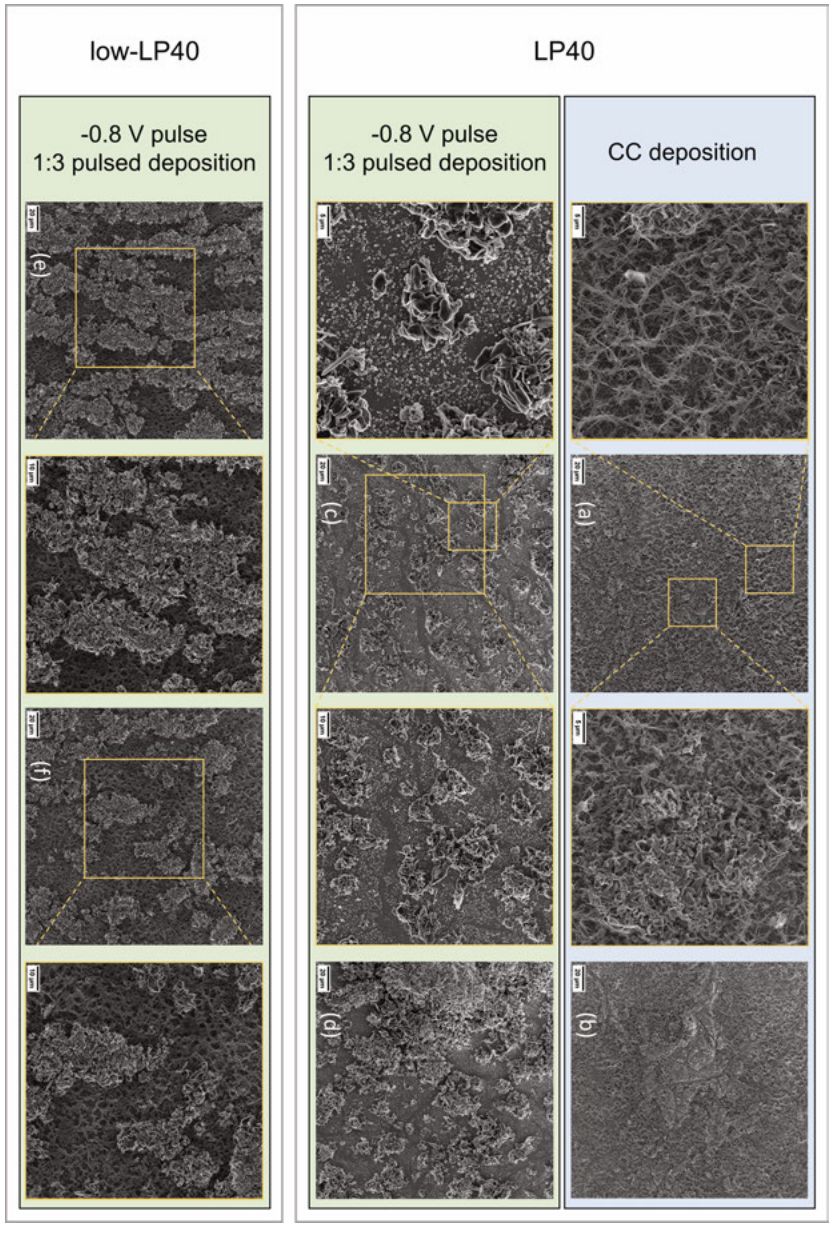

Figure 4.17. SEM images depicting the morphologies of the lithium deposits obtained on the pure copper substrates after the first deposition step in two electrolytes (i.e., LP40 and the low-LP40) using the different deposition protocols (see Section 3.1 and **Paper V** for more details). The total deposition charge was 0.5 mAh cm^{-2}. The current used for the CC deposition was 1.0 mA cm^{-2}. The pulsed-current deposition was carried out with current-on time and current-off (i.e., open-circuit) time of 1 and 3 ms, respectively. During the current-on time, a current of 1.0 mA cm^{-2} was used. Note that the nucleation pulse was followed by an open-circuit pause of 100 ms for the same reason as explained in Section 4.4.1.

According to the electrodeposition theory, providing a large overpotential e.g., via the use of a potentiostatic nucleation pulse with a sufficiently high pulse height, should result in a dramatic increase in the density of lithium nuclei on the electrode surface. This may enable instantaneous homogenous nucleation of a multitude of similarly sized lithium nuclei all over the copper surface and hence facilitate homogeneous deposition. Dramatically different deposition results without the formation of the lithium threads were indeed obtained when a potentiostatic pulse of -0.8 V was applied in combination with the pulsed-current deposition (see **Figure 4.17**c and d). Since the adopted pulsed-current deposition was found to not have a huge impact on the deposition result (see Section 4.5.2), the slightly improved spatial distribution and increased number of lithium islands can be attributed to the inclusion of the nucleation pulse that increased the lithium nuclei density on the copper surface. This clearly demonstrates the decisive role of lithium nucleation on the deposition. Nevertheless, lithium islands of various sizes were still observed, and their distribution on the surface was far from homogeneous.

There could be two main reasons for the experiment results discussed above. First, even with the applied potentiostatic nucleation pulse, it could be difficult to achieve a sufficiently high overpotential at the surface of the copper substrate in the 1.0 M $LiPF_6$ electrolyte since a very high current would be required to decrease the surface concentration of Li^+ sufficiently. Such a high current should give rise to a large iR drop, which means that the true overpotential attained may be too low to allow the generation of nuclei homogeneously on the entire copper surface. The second possible reason is that the diffusion of lithium into the copper substrate (which should be particularly evident for small lithium clusters (i.e., nuclei embryos)) may decrease the number of nuclei that actually "survive" on the surface after the nucleation pulse. This is naturally a problem since the purpose of the nucleation pulse is to homogeneously generate a multitude of similarly sized lithium nuclei on the surface which then can grow during the subsequent deposition step.

One way to address the first issue and hence to facilitate homogeneous nucleation of lithium on the copper surface could be to decrease the Li^+ concentration in the electrolyte, as was previously shown for lithium nucleation on LMEs.[67] With a lower Li^+ concentration it should be easier to realize a high overpotential since the Li^+ reduction current (and hence the iR drop) should be lower. An analogous lithium deposition experiment, including the use of a nucleation pulse of -0.8 V, was therefore carried out in the low-LP40 electrolyte (see **Figure 4.17**e and f). Based on the improved spatial density and distribution of lithium islands on the copper surface, it is reasonable to conclude that the nucleation process was improved when using the low-LP40 electrolyte (compare **Figure 4.17**e and f with a-d). This supports the first hypothesis that a higher overpotential should be possible to reach during the nucleation pulse when the electrolyte has a lower Li^+ concentration. However, homogeneous nucleation on the entire copper surface was clearly still not achieved,

which could have been due to the lithium diffusion mentioned above. Last but not the least, it is worth to recall that the lithium activity dependency of the deposition potential can complicate the deposition of lithium on copper and possibly the application of a nucleation pulse as well.

4.5.2 Improving lithium nucleation/deposition via chemical prelithiation of the copper current collectors

In order to test the hypothesis that the diffusion of lithium into the copper substrate affected the lithium nucleation, lithium deposition experiments were carried out with "prelithiated" copper substrates (see Section 3.1). The idea is that if the copper substrates can be "saturated" in advance, lithium nucleation/deposition should be free from the complication imposed by the diffusion phenomenon and hence significantly improved. This strategy is schematically illustrated in **Figure 4.18** and was inspired by a diffusion-controlled lithium trapping study of Rehnlund et al.[33] In that study, the authors found a significant amount of lithium in copper foil after it had been in contact with elemental lithium for one week at 50°C, indicating that copper could be "chemically lithiated". In **Paper V**, using ICP-AES, the average amount of lithium in the prelithiatied copper substrates was found to be 11.5 µg cm^{-2}.

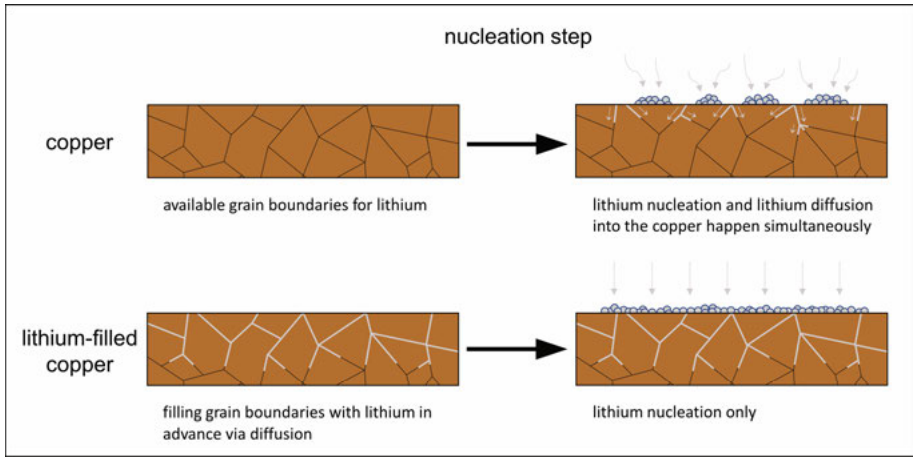

Figure 4.18. Schematic illustration of the proposed strategy in order to mitigate the influence of the lithium diffusion on nucleation.

As can be seen in **Figure 4.19**, dramatically improved deposition results were obtained with the prelithiated copper substrates. Using the prelithiated copper substrate and CC deposition in the absence of any nucleation pulse, the lithium deposits obtained in LP40 electrolyte were more compact and more densely distributed without any formation of loose networks of the lithium threads (compare **Figure 4.19**a with **4.17**a and b). This clearly demonstrates the

influence of the lithium diffusion into copper on the lithium nucleation on copper surface, in agreement with the abovementioned hypothesis. It is reasonable to propose that such diffusion was hindered due to the presence of lithium-saturated grain boundaries at the copper surface (see **Figure 4.18**). In **Figure 4.19**a, it can, however, still be seen that there were regions with less dense lithium deposits. The inhomogeneous deposition was not improved by using the pulsed-current deposition as can be seen in **Figure 4.19**b. This indicates that the adopted pulsed-current deposition had rather little impact on the deposition result in LP40 electrolyte as briefly mentioned above. More homogeneous deposition was, on the other hand, obtained when a potentiostatic nucleation pulse of -1.5 V was included prior to the pulsed-current deposition (see **Figure 4.19**c). This once again illustrates the decisive influence of the initial nucleation conditions. The experiment results consequently show that a poor nucleation step is unlikely to be compensated for using a subsequent pulsed-current deposition step, in good agreement with previous finding for lithium deposition on LMEs.[67]

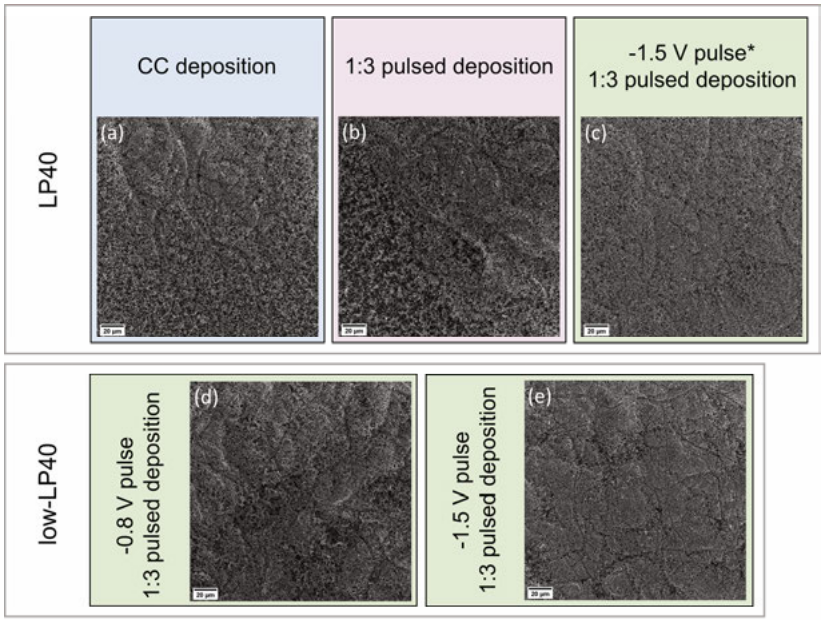

Figure 4.19. SEM images depicting the morphologies of the lithium deposits obtained on the prelithiated copper substrates after the first deposition step in two electrolytes (i.e., LP40 and the low-LP40) using the different deposition protocols (see Section 3.1 and **Paper V** for more details). The protocols are briefly described and explained in the caption of **Figure 4.17**. Note that the -1.5 V nucleation pulse could not be fully implemented in LP40 electrolyte (see the Supporting Information of **Paper V**).

Prelithiated copper substrates were also employed in lithium deposition experiments using the low-LP40 electrolyte. The clear difference between the

lithium morphologies obtained with a nucleation pulse of -0.8 V on the pure and prelithiated copper substrate (see **Figure 4.17**e and f and **4.19**d, respectively) indicates that the lithium diffusion into copper did affect the lithium nucleation conditions. Due to such diffusion, the potentiostatic nucleation pulse was ineffective for the pure copper substrates as the additionally-formed nuclei may simply be "consumed" by the substrates. The compact and homogeneous lithium deposits seen in **Figure 4.19**e, show that the nucleation and then growth of lithium on a prelithiated copper substrate could be further improved by increasing the pulse height of the nucleation pulse to -1.5 V. This is in good agreement with the nucleation hypothesis as a higher nuclei density (and hence a more homogeneous nucleation on the electrode surface) should be obtained when increasing the nucleation overpotential. Moreover, by comparing **Figure 4.19**c and e, it can also be concluded that the nucleation pulse was more efficient in conjunction with the low-LP40 electrolyte than with LP40 electrolyte. This can be ascribed to the higher overpotential that should be attained during the nucleation pulse in an electrolyte with a lower Li^+ concentration. Last but not the least, it should be noted that the pulse height of the potentiostatic nucleation pulse was limited to -0.8 V for the pure copper substrates due to the high current already generated/required. A potentiostatic nucleation pulse of -1.5 V could, on the other hand, be used with the prelithiated copper substrates. This may be explained by the fact that the lithium activity at the copper surface was increased by the prelithiation, which could have resulted in a decreased deposition current (see the Supporting Information of **Paper V** for more detailed discussion). The chemical prelithiation of the copper substrates hence not only improved the effectiveness of a nucleation pulse but also facilitated its application.

5. Conclusions and Outlook

This thesis focuses on two scientific problems that are related to the negative electrodes and/or negative electrode materials in lithium-based batteries (i.e., diffusion-controlled lithium trapping (**Paper I-III**) and inhomogeneous lithium deposition (**Paper IV** and **V**)).

In **Paper I**, the experiment results clearly demonstrate that a diffusion-controlled lithium trapping effect, analogous to that previously seen for negative electrodes based on alloy-forming materials, can also be seen for graphite electrodes. The diffusion-controlled trapping effect can be attributed to a two-way diffusion phenomenon, caused by the lithium concentration gradients generated in the electrode during lithiation, as a small fraction of the inserted lithium can diffuse too deeply to be extracted within the time domain of the subsequent delithiation step. It is demonstrated that the application of a CV delithiation step (following CC delithiation) can be used to extract some trapped lithium by driving further diffusion of lithium towards the electrode surface and thus improve the delithiation efficiency. By decreasing the influence of the trapping effect using the CV steps, graphite electrodes can have more stable electrochemical performances during cycling.

In **Paper II**, it is shown that the diffusion-controlled trapping of lithium in the graphite electrode can greatly affect the cycle life performance of NMC811/graphite full cells during 1C cycling. It is also shown that the conventional low-rate formation cycling is less effective in preparing cells for high-rate cycling. On the other hand, it is demonstrated that the CV step strategy proposed in **Paper I** can successfully mitigate the trapping effect and hence greatly improve the cell performance. However, by combining the results in **Paper I** and **II**, it is clear that CV delithiation or discharge steps can not be used arbitrarily since their appropriateness depends on the employed cycling rate and the lithium concentration profile in the graphite electrode. Nevertheless, **Paper I** and **II** clearly highlight the importance of considering the diffusion-controlled lithium trapping in graphite electrodes and to develop appropriate mitigation strategies.

In **Paper III**, it is concluded that the influence of the diffusion-controlled lithium trapping effect seen for silicon nanoparticle based electrodes can be affected by the employed silicon nanoparticle size, most likely via its influence on the electrode microstructure. Furthermore, on the basis of **Paper I** and **II**, it is important to realize that the cycling performances of the electrodes

should be determined by the dynamic and complex interplays between the employed lithiation and delithiation rates, the lithium concentration profile in the electrode, the microstructure of the electrode, the application of CV delithiation steps (if any), and the diffusion-controlled trapping effect.

In **Paper IV**, it is demonstrated that the inclusion of a potentiostatic stripping pulse of 4 V for 1 s before the first CC stripping step can enable the oxidative formation of homogeneously distributed and interconnected depressions which then can serve as preferential nucleation sites for lithium during the subsequent CC deposition step in conventional 1.0 M $LiPF_6$ electrolyte. The potentiostatic stripping pulse prevents lithium stripping from taking place only at the most electrochemically active sites on the LME surface by activating the entire surface via the formation of tiny pits. This results in a better controlled stripping process that then yields more homogenous lithium deposition and thus improved LME cycling stability and lifetime.

In **Paper V**, the experiment results demonstrate that the diffusion of lithium into copper current collectors can affect the lithium nucleation step and lead to inhomogeneous lithium deposition on the current collectors. The influence of this effect can, however, be decreased by chemically prelithiating the copper current collectors. The use of the prelithiated copper current collectors in combination with a potentiostatic nucleation pulse (e.g., -1.5 V for 10 ms) and an electrolyte with a low Li^+ concentration (e.g., 0.02 M) can facilitate the formation of a great number of homogeneously distributed nuclei on the surface, and thereby yield greatly improved lithium deposition. Overall, the results in **Paper IV** and **V** highlight the importance of considering the influence of the substrate and optimizing the nucleation step for lithium deposition.

In summary, studying and developing an improved understanding of the two scientific problems to find their potential solutions is a crucial step in the development of lithium-based batteries with longer cycling lifetimes and/or higher energy densities. As graphite is the dominating negative electrode material in contemporary lithium-ion batteries, the findings in **Paper I** and **II** should pave the way for new directions regarding studies of cell degradation and development of battery cell formation procedures. As silicon containing negative electrodes are being developed by battery manufacturers, such electrodes will most likely define the next-generation lithium-ion batteries. However, in order to succeed, proper electrode engineering and processing will be necessary, as implied by the findings in **Paper III**. Lithium-metal electrodes, especially in the “anode-free” configuration, can be considered as the ultimate negative electrodes for lithium-based batteries. Although the road ahead towards the commercial realization of lithium-metal batteries, particularly anode-free ones, may still be long, hopefully, the findings in **Paper IV** and **V** can provide some guidance.

Acknowledgments

Thank you, a lot, for reading this thesis. Even if this is the first page you check, I still thank you in advance for at least opening this thesis and hope you will find things that are interesting to you later.

So, this is it! It is really a long journey. Before I left Taiwan and came to Sweden in 2017, I never thought that I will one day become a doctor (well, hopefully, I will defend my thesis successfully).

First of all, Leif, without you giving me the opportunity, I would not have been here. I am always grateful for your guidance from the very beginning. Thank you for letting me have my own explorations without putting much pressure on me but enlightening me and providing me necessary support when I got stuck. Just like a good Dad!

Second, I would like to thank all the co-authors and people that were once involved in the projects in any way and percentage, including Ruijun Pan, David Rehnlund, Zhaohui Wang, Maria Paschalidou, Jean Pettersson, Heyin Chen, Christopher Joel Thulin, Yu-Chin Huang, Edvin Andersson, Yonas Tesfamhret, Anastasiia Mikheenkova, Yi-Chen Weng, Yu-Chuan Chien, Olof Gustafsson, Tatiana Koriukina, Haidong Liu, Alina Oltean, Fredrik Lindgren, Tamara Patranika, Khaled Mohammadi, Cuc Thu Mai, Saravanan Karuppiah, Guiomar Hernández, Robin Lundström, prof. Maria Hahlin, William Brant, Erik Lewin, Ignacio Cuevas, Florian Gebert… (Sorry, if I miss your name(s).)

To all the people in Structural Chemistry, I am sorry for not further naming anyone here. However, you should know that I am deeply filled with thankfulness. This journey would have been so much tougher and boring without you. It is my honor to have you in the last 4-5 years.

Thank you, Mengru, for your love, company and support, especially during the most difficult part of the journey. Last, but most importantly, my greatest gratitude of course goes to my parents and sister. Thank you for always being the strongest backing no matter what happens.

Now… It is time for me to submit the thesis… The clock is ticking…

Populärvetenskaplig sammanfattning

Uppfinnandet och den efterföljande utvecklingen av litiumbaserade batterier, särskilt litiumjonbatterier, har dramatiskt förändrat våra liv genom att möjliggöra en rad olika batteribaserade teknologier som smarta telefoner, bärbara datorer och elbilar. Men hur fungerar ett litiumjonbatteri? Dagens litiumjonbatterier är huvudsakligen uppbyggda av en positiv och en negativ elektrod som är åtskilda av ett poröst plast-membran indränkt med minst ett organiskt lösningsmedel innehållande ett litiumsalt. Den negativa elektroden består vanligtvis av grafit medan den positiva elektroden innehåller metalloxider. Batterierna tillverkas vanligtvis i urladdat tillstånd i vilket endast den positiva elektroden innehåller litiumjoner. Vid laddning sker elektrokemiska reaktioner (reduktion vid den negativa elektroden och oxidation vid den positiva elektroden) vilka leder till att litiumjoner och elektroner förflyttas från den positiva elektroden till den ursprungligen tomma negativa elektroden. De laddade batterierna kan sedan användas för att driva olika elektroniska apparater, under det att litiumjoner förflyttas från den negativa elektro-den tillbaka till den positiva elektroden som en följd av att de elektro-kemiska processerna då spontant går i omvänd riktning.

En annan typ av litiumbaserade batterier är litiummetallbatterier. Ett sådant batteri har i princip samma sammansättning som den som beskrivits ovan bortsett från att den negativa elektroden nu i stället består av metalliskt litium i stället för grafit. Användningen av litiummetallelektroder gör att energitätheten för batteriet ökar kraftigt. I ett litiummetallbatteri reduceras litiumjoner till metalliskt litium på den negativa elektroden vid laddningen av batteriet. Vid urladdningen så återbildas litiumjoner ge-nom att litiummetallelektroden oxideras varvid litiumjoner bildas. Litiumjoner och elektroner rör sig då till den positiva elektroden.

Den fortsatta utvecklingen av de teknologier som först möjliggjordes av litiumbaserade batterier, som till exempel utvecklingen av dagens elbilar, har skapat ett behov av allt bättre litiumbaserade batterier med högre och högre energitäthet och längre och längre livslängder. För att kunna möta dessa krav finns det ett behov av grundläggande studier av hur negativa elektroder fungerar. En viktig uppgift handlar om att bygga upp en mer fullständig förståelse av alla de fenomen som begränsar de negativa elektrodernas prestanda. För att kunna förlänga livslängden för litiumbaserade batterier krävs det också förbättrade strategier för att bemöta effekten av olika fenomen. Men för att kunna

ta fram sådana strategier måste man veta vilket fenomen som utgör det viktigaste problemet.

I denna avhandling har två vetenskapliga problem relaterade till olika negativa elektroder studerats.

Det första problemet handlar om att en del av litiumjonerna fastnar i den negativa elektroden när man använder litiumjonbatterierna. Detta gör att batteriets kapacitet minskar med tiden eftersom batteriets funktion bygger på att alla litiumjoner kan röra sig fram och tillbaka mellan den positiva och den negativa elektroden. Det har nyligen visats att en liten del av de litiumjoner som åker in i den negativa elektroden under uppladdningen av batteriet stannar kvar i elektroden även efter urladdningen. Detta sker eftersom litiumjonerna kan röra sig för långt in i elektroden för att hinna lämna elektroden i tid under urladdningen. Eftersom denna process upprepas varje gång som batteriet laddas upp så kommer inverkan av denna effekt inte att märkas förrän ett visst antal uppladdningar har gjorts. I den första delen av avhandlingen studeras denna effekt för negativa elektroder baserade antingen på grafit eller kisel. Syftet var här att förbättra förståelsen av denna relativt nyupptäckta kapacitetsförlust-effekt och att utveckla strategier för att minimera dess påverkan på olika batterier. Ett exempel på en sådan strategi, som beskrivs i avhandlingen, är att göra det lättare att dra ut de infångade litiumjonerna med hjälp av en pålagd spänning.

Det andra problemet som behandlas i avhandlingen handlar om att litium inte deponeras homogent på den negativa elektroden i litiummetallbatterier under uppladdningsprocessen. Detta gör att litiummetallelektrodens yta blir mer och mer porös med tiden vilket ökar risken för att litiumtrådar (dendriter) ska bildas. Då dessa trådar kan kortsluta batteriet kan detta innebära stora säkerhetsrisker. Detta är faktiskt en viktig orsak till att litiummetallbatterier inte används i någon större utsträckning idag. Anledningen till att deponeringen av litium inte sker homogent på elektrodens yta är att litiumet tenderar att deponeras på de platser på elektrodytan som är speciellt lätta att deponera på och att den efterföljande deponeringen sedan fortsätter på samma ställe. En följd av detta är att litiummetallbatterier i regel har mycket begränsade livslängder. I den andra delen av avhandlingen beskrivs försök att utveckla strategier för att förbättra både litiumdepositions- och litiumupplösningsprocessen genom att förändra elektrodens yta, återigen med hjälp av en pålagd spänning.

References

[1] G.N. Lewis, F.G. Keyes, *J. Am. Chem. Soc.* **1913**, *35*, 340.
[2] M. Winter, B. Barnett, K. Xu, *Chem. Rev.* **2018**, *118*, 11433.
[3] J.B. Goodenough, K.S. Park, *J. Am. Chem. Soc.* **2013**, *135*, 1167.
[4] J.B. Goodenough, Y. Kim, *Chem. Mater.* **2010**, *22*, 587.
[5] E. Peled, S. Menkin, *J. Electrochem. Soc.* **2017**, *164*, A1703.
[6] M.B. Pinson, M.Z. Bazant, *J. Electrochem. Soc.* **2013**, *160*, A243.
[7] C.R. Birkl, M.R. Roberts, E. McTurk, P.G. Bruce, D.A. Howey, *J. Power Sources* **2017**, *341*, 373.
[8] A.J. Smith, J.C. Burns, D. Xiong, J.R. Dahn, *J. Electrochem. Soc.* **2011**, *158*, A1136.
[9] A. Wang, S. Kadam, H. Li, S. Shi, Y. Qi, *Npj Comput. Mater.* **2018**, *4*, 15.
[10] J.S. Edge, S. O'Kane, R. Prosser, N.D. Kirkaldy, A.N. Patel, A. Hales, A. Ghosh, W. Ai, J. Chen, J. Yang, S. Li, M.C. Pang, L. Bravo Diaz, A. Tomaszewska, M.W. Marzook, K.N. Radhakrishnan, H. Wang, Y. Patel, B. Wu, G.J. Offer, *Phys. Chem. Chem. Phys.* **2021**, *23*, 8200.
[11] T. Li, X.Z. Yuan, L. Zhang, D. Song, K. Shi, C. Bock, *Electrochem. Energy Rev.* **2020**, *3*, 43.
[12] M. Weiss, R. Ruess, J. Kasnatscheew, Y. Levartovsky, N.R. Levy, P. Minnmann, L. Stolz, T. Waldmann, M. Wohlfahrt-Mehrens, D. Aurbach, M. Winter, Y. Ein-Eli, J. Janek, *Adv. Energy Mater.* **2021**, *11*, 2101126.
[13] P.M. Attia, A. Bills, F. Brosa Planella, P. Dechent, G. dos Reis, M. Dubarry, P. Gasper, R. Gilchrist, S. Greenbank, D. Howey, O. Liu, E. Khoo, Y. Preger, A. Soni, S. Sripad, A.G. Stefanopoulou, V. Sulzer, *J. Electrochem. Soc.* **2022**, *169*, 060517.
[14] Y. Liu, Y. Zhu, Y. Cui, *Nat. Energy* **2019**, *4*, 540.
[15] X. Han, L. Lu, Y. Zheng, X. Feng, Z. Li, J. Li, M. Ouyang, *ETransportation* **2019**, *1*, 100005.
[16] J.P. Pender, G. Jha, D.H. Youn, J.M. Ziegler, I. Andoni, E.J. Choi, A. Heller, B.S. Dunn, P.S. Weiss, R.M. Penner, C.B. Mullins, *ACS Nano* **2020**, *14*, 1243.
[17] P.N. Suryadi, J. Karunawan, O. Floweri, F. Iskandar, *J. Energy Storage* **2023**, *68*, 107634.
[18] R. Xiong, Y. Pan, W. Shen, H. Li, F. Sun, *Renew. Sustain. Energy Rev.* **2020**, *131*, 110048.
[19] J.G. Qu, Z.Y. Jiang, J.F. Zhang, *J. Energy Storage* **2022**, *52*, 104811.
[20] M.N. Obrovac, L. Christensen, *Electrochem. Solid-State Lett.* **2004**, *7*, A93.
[21] J. Guo, D. Dong, J. Wang, D. Liu, X. Yu, Y. Zheng, Z. Wen, W. Lei, Y. Deng, J. Wang, G. Hong, H. Shao, *Adv. Funct. Mater.* **2021**, *31*, 2102546.
[22] S. Chae, M. Ko, K. Kim, K. Ahn, J. Cho, *Joule* **2017**, *1*, 47.
[23] M.N. Obrovac, L. Christensen, D.B. Le, J.R. Dahn, *J. Electrochem. Soc.* **2007**, *154*, A849.
[24] A. Casimir, H. Zhang, O. Ogoke, J.C. Amine, J. Lu, G. Wu, *Nano Energy* **2016**, *27*, 359.

[25] K. Feng, M. Li, W. Liu, A.G. Kashkooli, X. Xiao, M. Cai, Z. Chen, *Small* **2018**, *14*, 1702737.
[26] Z. Chen, A. Soltani, Y. Chen, Q. Zhang, A. Davoodi, S. Hosseinpour, W. Peukert, W. Liu, *Adv. Energy Mater.* **2022**, *12*, 2200924.
[27] M.N. Obrovac, V.L. Chevrier, *Chem. Rev.* **2014**, *114*, 11444.
[28] C. Gan, C. Zhang, W. Wen, Y. Liu, J. Chen, Q. Xie, X. Luo, *ACS Appl. Mater. Interfaces* **2019**, *11*, 35809.
[29] Z. Ma, T. Li, Y.L. Huang, J. Liu, Y. Zhou, D. Xue, *RSC Adv.* **2013**, *3*, 7398.
[30] X.H. Liu, L. Zhong, S. Huang, S.X. Mao, T. Zhu, J.Y. Huang, *ACS Nano* **2012**, *6*, 1522.
[31] R. V. Salvatierra, W. Chen, J.M. Tour, *Adv. Energy Sustain. Res.* **2021**, *2*, 2000110.
[32] S. Nanda, A. Gupta, A. Manthiram, *Adv. Energy Mater.* **2021**, *11*, 2000804.
[33] D. Rehnlund, F. Lindgren, S. Böhme, T. Nordh, Y. Zou, J. Pettersson, U. Bexell, M. Boman, K. Edström, L. Nyholm, *Energy Environ. Sci.* **2017**, *10*, 1350.
[34] F. Lindgren, D. Rehnlund, R. Pan, J. Pettersson, R. Younesi, C. Xu, T. Gustafsson, K. Edström, L. Nyholm, *Adv. Energy Mater.* **2019**, *9*, 1901608.
[35] D. Rehnlund, Z. Wang, L. Nyholm, *Adv. Mater.* **2022**, *34*, 2108827.
[36] Q. Ai, D. Li, J. Guo, G. Hou, Q. Sun, Q. Sun, X. Xu, W. Zhai, L. Zhang, J. Feng, P. Si, J. Lou, L. Ci, *Adv. Mater. Interfaces* **2019**, *6*, 1901187.
[37] B. Zhu, G. Liu, G. Lv, Y. Mu, Y. Zhao, Y. Wang, X. Li, P. Yao, Y. Deng, Y. Cui, J. Zhu, *Sci. Adv.* **2019**, *5*, eaax0651.
[38] J. Xiong, N. Dupré, P. Moreau, B. Lestriez, *Adv. Energy Mater.* **2022**, *12*, 2103348.
[39] B. Sreenarayanan, D.H.S. Tan, S. Bai, W. Li, W. Bao, Y.S. Meng, *J. Power Sources* **2022**, *531*, 231327.
[40] Y. Li, X. Zheng, Z. Cao, Y. Wang, Y. Wang, L. Lv, W. Huang, Y. Huang, H. Zheng, *Energy Storage Mater.* **2023**, *55*, 660.
[41] P.J. Crowley, K.P. Scanlan, A. Manthiram, *J. Power Sources* **2022**, *546*, 231973.
[42] C. von Lüders, V. Zinth, S. V. Erhard, P.J. Osswald, M. Hofmann, R. Gilles, A. Jossen, *J. Power Sources* **2017**, *342*, 17.
[43] L.J. Hardwick, H. Buqa, P. Novák, *Solid State Ionics* **2006**, *177*, 2801.
[44] K.E. Thomas-Alyea, C. Jung, R.B. Smith, M.Z. Bazant, *J. Electrochem. Soc.* **2017**, *164*, E3063.
[45] A. Senyshyn, M.J. Mühlbauer, O. Dolotko, M. Hofmann, H. Ehrenberg, *Sci. Rep.* **2015**, *5*, 18380.
[46] Y. Reynier, R. Yazami, B. Fultz, *J. Power Sources* **2007**, *165*, 616.
[47] Y. Li, M. Bettge, B. Polzin, Y. Zhu, M. Balasubramanian, D.P. Abraham, *J. Electrochem. Soc.* **2013**, *160*, 3006.
[48] E.J. McShane, A.M. Colclasure, D.E. Brown, Z.M. Konz, B.D. McCloskey, *ACS Energy Lett.* **2020**, *5*, 2045.
[49] K.P.C. Yao, J.S. Okasinski, K. Kalaga, I.A. Shkrob, D.P. Abraham, *Energy Environ. Sci.* **2019**, *12*, 656.
[50] A. Senyshyn, M.J. Mühlbauer, K. Nikolowski, T. Pirling, H. Ehrenberg, *J. Power Sources* **2012**, *203*, 126.
[51] S.A. Krachkovskiy, J.M. Foster, J.D. Bazak, B.J. Balcom, G.R. Goward, *J. Phys. Chem. C* **2018**, *122*, 21784.
[52] D.P. Finegan, A. Quinn, D.S. Wragg, A.M. Colclasure, X. Lu, C. Tan, T.M.M. Heenan, R. Jervis, D.J.L. Brett, S. Das, T. Gao, D.A. Cogswell, M.Z. Bazant,

M. Di Michiel, S. Checchia, P.R. Shearing, K. Smith, *Energy Environ. Sci.* **2020**, *13*, 2570.
[53] M. Gyanprakash D., C. Kumar Rastogi, *J. Electroanal. Chem.* **2023**, *931*, 117176.
[54] C. Keller, A. Desrues, S. Karuppiah, E. Martin, J.P. Alper, F. Boismain, C. Villevieille, N. Herlin-Boime, C. Haon, P. Chenevier, *Nanomaterials* **2021**, *11*, 307.
[55] M. Boniface, L. Quazuguel, J. Danet, D. Guyomard, P. Moreau, P. Bayle-Guillemaud, *Nano Lett.* **2016**, *16*, 7381.
[56] J. Yu, K. Wang, W. Song, H. Huang, C. Liang, Y. Xia, J. Zhang, Y. Gan, F. Wang, W. Zhang, *Chem. Eng. J.* **2021**, *406*, 126805.
[57] K. Feng, M. Li, W. Liu, A.G. Kashkooli, X. Xiao, M. Cai, Z. Chen, *Small* **2018**, *14*, 1702737.
[58] H. Wang, X. Ji, C. Chen, K. Xu, L. Miao, *AIP Adv.* **2013**, *3*, 112102.
[59] R. Greff, R. Peat, L.M. Peter, D. Pletcher, J. Robinson, *Instrumental Methods in Electrochemistry*, Ellis Horwood **1990**.
[60] M. Paunovic, M. Schlesinger, *Fundamentals of Electrochemical Deposition*, Wiley **1998**.
[61] J. Mostany, B.R. Scharifker, K. Saavedra, C. Borrás, *Russ. J. Electrochem.* **2008**, *44*, 652.
[62] Y.S. Cohen, Y. Cohen, D. Aurbach, *J. Phys. Chem. B* **2000**, *104*, 12282.
[63] K.N. Wood, E. Kazyak, A.F. Chadwick, K.H. Chen, J.G. Zhang, K. Thornton, N.P. Dasgupta, *ACS Cent. Sci.* **2016**, *2*, 790.
[64] X.Q. Zhang, X.B. Cheng, Q. Zhang, *Adv. Mater. Interfaces* **2018**, *5*, 1701097.
[65] S. Li, M. Jiang, Y. Xie, H. Xu, J. Jia, J. Li, *Adv. Mater.* **2018**, *30*, 1706375.
[66] K.N. Wood, M. Noked, N.P. Dasgupta, *ACS Energy Lett.* **2017**, *2*, 664.
[67] D. Rehnlund, C. Ihrfors, J. Maibach, L. Nyholm, *Mater. Today* **2018**, *21*, 1010.
[68] H. Liu, X. Cheng, R. Xu, X. Zhang, C. Yan, J. Huang, *Adv. Energy Mater.* **2019**, *9*, 1902254.
[69] A.J. Sanchez, E. Kazyak, Y. Chen, K.H. Chen, E.R. Pattison, N.P. Dasgupta, *ACS Energy Lett.* **2020**, *5*, 994.
[70] K.H. Chen, K.N. Wood, E. Kazyak, W.S. Lepage, A.L. Davis, A.J. Sanchez, N.P. Dasgupta, *J. Mater. Chem. A* **2017**, *5*, 11671.
[71] X.B. Cheng, R. Zhang, C.Z. Zhao, Q. Zhang, *Chem. Rev.* **2017**, *117*, 10403.
[72] Y. Zhang, T.T. Zuo, J. Popovic, K. Lim, Y.X. Yin, J. Maier, Y.G. Guo, *Mater. Today* **2020**, *33*, 56.
[73] B. Horstmann, J. Shi, R. Amine, M. Werres, X. He, H. Jia, F. Hausen, I. Cekic-Laskovic, S. Wiemers-Meyer, J. Lopez, D. Galvez-Aranda, F. Baakes, D. Bresser, C.-C. Su, Y. Xu, W. Xu, P. Jakes, R.-A. Eichel, E. Figgemeier, U. Krewer, J.M. Seminario, P.B. Balbuena, C. Wang, S. Passerini, Y. Shao-Horn, M. Winter, K. Amine, R. Kostecki, A. Latz, *Energy Environ. Sci.* **2021**, *14*, 5289.
[74] R. Zhang, X.B. Cheng, C.Z. Zhao, H.J. Peng, J. Le Shi, J.Q. Huang, J. Wang, F. Wei, Q. Zhang, *Adv. Mater.* **2016**, *28*, 2155.
[75] S.-S. Chi, Y. Liu, W.-L. Song, L.-Z. Fan, Q. Zhang, *Adv. Funct. Mater.* **2017**, *27*, 1700348.
[76] L. Chen, J.G. Connell, A. Nie, Z. Huang, K.R. Zavadil, K.C. Klavetter, Y. Yuan, S. Sharifi-Asl, R. Shahbazian-Yassar, J.A. Libera, A.U. Mane, J.W. Elam, *J. Mater. Chem. A* **2017**, *5*, 12297.
[77] E. Kazyak, K.N. Wood, N.P. Dasgupta, *Chem. Mater.* **2015**, *27*, 6457.
[78] W. Li, H. Yao, K. Yan, G. Zheng, Z. Liang, Y.M. Chiang, Y. Cui, *Nat. Commun.* **2015**, *6*, 7436.

[79] X.Q. Zhang, X.B. Cheng, X. Chen, C. Yan, Q. Zhang, *Adv. Funct. Mater.* **2017**, *27*, 1605989.
[80] S. Xiong, L. Nyholm, A. Matic, C. Zhang, *Mater. Today Energy* **2022**, *28*, 101060.
[81] Z. Xie, Z. Wu, X. An, X. Yue, J. Wang, A. Abudula, G. Guan, *Energy Storage Mater.* **2020**, *32*, 386.
[82] M. Gao, H. Li, L. Xu, Q. Xue, X. Wang, Y. Bai, C. Wu, *J. Energy Chem.* **2021**, *59*, 666.
[83] H. Yuan, X. Ding, T. Liu, J. Nai, Y. Wang, Y. Liu, C. Liu, X. Tao, *Mater. Today* **2022**, *53*, 173.
[84] A.J. Louli, A. Eldesoky, R. Weber, M. Genovese, M. Coon, J. DeGooyer, Z. Deng, R.T. White, J. Lee, T. Rodgers, R. Petibon, S. Hy, S.J.H. Cheng, J.R. Dahn, *Nat. Energy* **2020**, *5*, 693.
[85] R. Weber, M. Genovese, A.J. Louli, S. Hames, C. Martin, I.G. Hill, J.R. Dahn, *Nat. Energy* **2019**, *4*, 683.
[86] S. Jurng, Z.L. Brown, J. Kim, B.L. Lucht, *Energy Environ. Sci.* **2018**, *11*, 2600.
[87] J. Qian, W.A. Henderson, W. Xu, P. Bhattacharya, M. Engelhard, O. Borodin, J.G. Zhang, *Nat. Commun.* **2015**, *6*, 6362.
[88] D.W. Kang, J. Moon, H.Y. Choi, H.C. Shin, B.G. Kim, *J. Power Sources* **2021**, *490*, 229504.
[89] C. Yan, Y.-X. Yao, X. Chen, X.-B. Cheng, X.-Q. Zhang, J.-Q. Huang, Q. Zhang, *Angew. Chemie* **2018**, *130*, 14251.
[90] D. Liu, X. Xiong, Q. Liang, X. Wu, H. Fu, *Chem. Commun.* **2021**, *57*, 9232.
[91] S. Liu, X. Ji, N. Piao, J. Chen, N. Eidson, J. Xu, P. Wang, L. Chen, J. Zhang, T. Deng, S. Hou, T. Jin, H. Wan, J. Li, J. Tu, C. Wang, *Angew. Chemie - Int. Ed.* **2021**, *60*, 3661.
[92] H. Zhao, D. Lei, Y.B. He, Y. Yuan, Q. Yun, B. Ni, W. Lv, B. Li, Q.H. Yang, F. Kang, J. Lu, *Adv. Energy Mater.* **2018**, *8*, 1800266.
[93] X. Ma, Z. Liu, H. Chen, *Nano Energy* **2019**, *59*, 500.
[94] P. Zhai, Y. Wei, J. Xiao, W. Liu, J. Zuo, X. Gu, W. Yang, S. Cui, B. Li, S. Yang, Y. Gong, *Adv. Energy Mater.* **2020**, *10*, 1903339.
[95] A.A. Assegie, C.C. Chung, M.C. Tsai, W.N. Su, C.W. Chen, B.J. Hwang, *Nanoscale* **2019**, *11*, 2710.
[96] R. Zhang, X.R. Chen, X. Chen, X.B. Cheng, X.Q. Zhang, C. Yan, Q. Zhang, *Angew. Chemie - Int. Ed.* **2017**, *56*, 7764.
[97] K. Yan, Z. Lu, H. Lee, F. Xiong, P. Hsu, Y. Li, J. Zhao, S. Chu, Y. Cui, *Nat. Energy* **2016**, *1*, 16010.
[98] N. Xu, L. Li, Y. He, Y. Tong Y. Lu, *J. Mater. Chem. A* **2020**, *8*, 6229.
[99] J. Qian, S. Wang, Y. Li, M. Zhang, F. Wang, Y. Zhao, Q. Sun, L. Li, F. Wu, R. Chen, *Adv. Funct. Mater.* **2021**, *31*, 2006950.
[100] N. Zhang, S.H. Yu, H.D. Abruña, *Chem. Commun.* **2019**, *55*, 10124.
[101] N. Zhang, S.H. Yu, H.D. Abruña, *Nano Res.* **2020**, *13*, 45.
[102] D. Rehnlund, J. Pettersson, K. Edström, L. Nyholm, *ChemistrySelect* **2018**, *3*, 2311.
[103] S. Lv, T. Verhallen, A. Vasileiadis, F. Ooms, Y. Xu, Z. Li, Z. Li, M. Wagemaker, *Nat. Commun.* **2018**, *9*, 2152.
[104] R. Rupp, B. Caerts, A. Vantomme, J. Fransaer, A. Vlad, *J. Phys. Chem. Lett.* **2019**, *10*, 5206.
[105] F. Linsenmann, M. Trunk, P. Rapp, L. Werner, R. Gernhäuser, R. Gilles, B. Märkisch, Z. Révay, H.A. Gasteiger, *J. Electrochem. Soc.* **2020**, *167*, 100554.
[106] H. Okamoto, *J. Phase Equilibria Diffus.* **2011**, *32*, 172.

[107] A. Vlad, A.L.M. Reddy, A. Ajayan, N. Singh, J.F. Gohy, S. Melinte, P.M. Ajayan, *Proc. Natl. Acad. Sci. U. S. A.* **2012**, *109*, 15168.
[108] Y. Liu, M. Sun, Y. Yuan, Q. Wu, H. Wang, Y. He, Z. Lin, F. Zhou, M. Ling, C. Qian, C. Liang, J. Lu, *Adv. Funct. Mater.* **2020**, *30*, 1910249.
[109] V.A. Sethuraman, K. Kowolik, V. Srinivasan, *J. Power Sources* **2011**, *196*, 393.
[110] M.J. Lacey, K. Edström, D. Brandell, *Chem. Commun.* **2015**, *51*, 16502.
[111] M.J. Lacey, *ChemElectroChem* **2017**, *4*, 1997.
[112] Y.C. Chien, A.S. Menon, W.R. Brant, D. Brandell, M.J. Lacey, *J. Am. Chem. Soc.* **2020**, *142*, 1449.
[113] R. de Levie, *Electrochim. Acta* **1963**, *8*, 751.
[114] A.J. Bard, L.R. Faulkner, *Electrochemical Methods: Fundamentals and Applications, 2nd Edition*, Wiley **2000**.
[115] H.J. Ploehn, P. Ramadass, R.E. White, *J. Electrochem. Soc.* **2004**, *151*, A456.
[116] A. Barai, G.H. Chouchelamane, Y. Guo, A. McGordon, P. Jennings, *J. Power Sources* **2015**, *280*, 74.
[117] F.M. Kindermann, A. Noel, S. V. Erhard, A. Jossen, *Electrochim. Acta* **2015**, *185*, 107.
[118] P.J. Osswald, S. V. Erhard, A. Rheinfeld, B. Rieger, H.E. Hoster, A. Jossen, *J. Power Sources* **2016**, *329*, 546.
[119] Y.-K. Huang, J. Pettersson, L. Nyholm, *Adv. Energy Sustain. Res.* **2022**, *3*, 2200042.
[120] C. Zhao, T. Wada, V. De Andrade, D. Gürsoy, H. Kato, Y. K. Chen-Wiegart, *Nano Energy* **2018**, *52*, 381.
[121] A.L. Michan, G. Divitini, A.J. Pell, M. Leskes, C. Ducati, C.P. Grey, *J. Am. Chem. Soc.* **2016**, *138*, 7918.
[122] G. Zhu, D. Chao, W. Xu, M. Wu, H. Zhang, *ACS Nano* **2021**, *15*, 15567.
[123] Y. Lee, T. Lee, J. Hong, J. Sung, N. Kim, Y. Son, J. Ma, S.Y. Kim, J. Cho, *Adv. Funct. Mater.* **2020**, *30*, 2004841.
[124] L. Gireaud, S. Grugeon, S. Laruelle, B. Yrieix, J.M. Tarascon, *Electrochem. Commun.* **2006**, *8*, 1639.
[125] M.S. Chandrasekar, M. Pushpavanam, *Electrochim. Acta* **2008**, *53*, 3313.
[126] J. Fleig, J. Maier, *J. Electroceramics* **1997**, *1*, 73.
[127] B. Wu, J. Lochala, T. Taverne, J. Xiao, *Nano Energy* **2017**, *40*, 34.
[128] Y.K. Huang, R. Pan, D. Rehnlund, Z. Wang, L. Nyholm, *Adv. Energy Mater.* **2021**, *11*, 2003674.

Acta Universitatis Upsaliensis

Digital Comprehensive Summaries of Uppsala Dissertations from the Faculty of Science and Technology 2339

Editor: The Dean of the Faculty of Science and Technology

A doctoral dissertation from the Faculty of Science and Technology, Uppsala University, is usually a summary of a number of papers. A few copies of the complete dissertation are kept at major Swedish research libraries, while the summary alone is distributed internationally through the series Digital Comprehensive Summaries of Uppsala Dissertations from the Faculty of Science and Technology. (Prior to January, 2005, the series was published under the title "Comprehensive Summaries of Uppsala Dissertations from the Faculty of Science and Technology".)

Distribution: publications.uu.se
urn:nbn:se:uu:diva-516251

ACTA UNIVERSITATIS
UPSALIENSIS
2023